How Does Vegetation Movement During Laser Scanning Affect Common Point Cloud-Derived Metrics? A Virtual Laser Scanning Study

Master's Thesis of

Hannah Weiser

2023-05-19

at the Faculty of Chemistry and Earth Sciences
Institute of Geography
Heidelberg University

Reviewer:	Prof. Dr. Bernhard Höfle
Second reviewer:	Prof. Dr. Fabian Fassnacht

STATUTORY DECLARATION

I declare that I have authored this thesis independently, that I have not used other than the declared sources / resources and that I have explicitly marked all material which has been quoted either literally or by content from the used sources.

This paper was not previously presented to another examination board and has not been published.

EIDESSTATTLICHE ERKLÄRUNG

Hiermit versichere ich, dass ich die vorliegende Arbeit selbstständig verfasst und keine anderen als die angegebenen Quellen und Hilfsmittel benutzt habe. Alle Ausführungen, die anderen veröffentlichten oder nicht veröffentlichten Schriften wörtlich oder sinngemäß entnommen wurden, habe ich kenntlich gemacht.

Die Arbeit hat in gleicher oder ähnlicher Fassung noch keiner anderen Prüfungsbehörde vorgelegen.

Heidelberg, 2023-05-19

H. Weiser

.....

(Hannah Weiser)

Acknowledgements

I would like to express my sincere appreciation to Prof. Bernhard Höfle, my supervisor, for developing the idea with me and for providing invaluable advice, guidance and support throughout the process.

Furthermore, I extend my gratitude to Prof. Fabian Fassnacht, my colleagues, and all participants of the research seminar for their constructive feedback when I presented my idea and progress. I would like to give special recognition to Alberto for the software-related assistance, and to Vivi and Katharina for the valuable discussions and for helping to polish my thesis through their careful review.

Finally, I would like to thank my friends for helping me stay relaxed and balanced, and, most importantly, my family for their unconditional support and encouragement throughout my academic journey so far.

Abstract

Close-range, high-resolution laser scanning is used in ecology, forestry and precision agriculture to assess plant health, structure, and productivity, and to monitor growth or regular movement patterns. A common problem in these applications is the wind-induced movement of vegetation during the scanning process, which can lead to multiple representations or blurring of leaves and branches. In this work, we investigate how leaf motion affects common metrics derived from high-resolution terrestrial and UAV-borne laser scanning point clouds of small apple trees. To this end, we use virtual laser scanning of synthetic trees with different levels of animated leaf flutter. Height metrics, voxel metrics, geometric features, and leaf area are calculated from the simulated single-tree laser scanning point clouds and compared across the motion scenarios. Furthermore, the effects of point cloud filtering on terrestrial laser scanning (TLS) data are quantified, both using virtual laser scanning point clouds and a real laser scanning point cloud. We found that leaf motion has significant effects on metrics derived from TLS point clouds, such as the number of leaf and wood points, voxel-based metrics, and geometric features. Leaf area is increasingly overestimated by direct geometric methods as leaf motion increases, with errors up to five times higher than without leaf motion. Meanwhile, standard height metrics and indirect light-extinction based leaf area estimates are fairly robust to leaf flutter. Modelled leaf movement also does not affect the metrics derived from simulated UAV-borne laser scanning point clouds. Leaf area estimation from TLS point clouds using geometric methods can be improved by applying a moving least squares surface approximation filter, which reduces measurement noise and motion effects. This study demonstrates how virtual laser scanning can be used to systematically investigate variables that influence the laser scanning result. Furthermore, by modelling trees as dynamic 3D objects, we take a step towards more realistic simulated point clouds, making virtual laser scanning a powerful method for developing algorithms to analyse 4D vegetation time series.

Zusammenfassung

Hochauflösendes Laserscanning im Nahbereich wird in der Ökologie, der Forstwirtschaft und der Präzisionslandwirtschaft eingesetzt, um die Gesundheit, Struktur und Produktivität von Pflanzen zu beurteilen und ihr Wachstum oder regelmäßige Bewegungsmuster nachzuvollziehen. Ein häufiges Problem bei diesen Anwendungen ist die windbedingte Bewegung der Vegetation während des Scanvorgangs, die zu Mehrfachdarstellungen oder Unschärfe von Blättern und Ästen führen kann. In dieser Arbeit untersuchen wir den Einfluss von Blattbewegung auf gängige Metriken, die aus hochauflösenden terrestrischen und UAV-basierten Laserscan-Punktwolken kleiner Apfelbäume abgeleitet werden. Zu diesem Zweck verwenden wir virtuelles Laserscanning von synthetischen Bäumen mit verschiedenen Szenarien animierter Blattschwingungen. Aus den simulierten Laserscanning-Punktwolken der einzelnen Bäume werden Höhenmetriken, Voxelmetriken, geometrische Features und die Blattfläche berechnet und über die Bewegungsszenarien hinweg verglichen. Darüber hinaus werden die Auswirkungen von Punktwolkenfiltern auf terrestrische Laserscanning (TLS)-Daten quantifiziert, wofür sowohl virtuelle als auch eine reale Laserscanning-Punktwolke verwendet werden. Wir fanden heraus, dass Blattbewegungen signifikante Auswirkungen auf Metriken haben, die aus TLS-Punktwolken abgeleitet wurden, darunter die Anzahl der Blatt- und Holzpunkte, voxelbasierte Metriken und geometrische Features. Die Blattfläche wird mit stärkerer Blattbewegung durch direkte geometrische Methoden zunehmend überschätzt, wobei die Fehler bis zu fünfmal höher sind als ohne Blattbewegung. Dem gegenüber sind Standard-Höhenmetriken und indirekte, auf Extinktion von Licht basierende Schätzungen der Blattfläche recht robust gegenüber Blattschwingungen. Die modellierte Blattbewegung wirkt sich auch nicht nennenswert auf Metriken aus, die aus simulierten UAV-gestützten Laserscanning-Punktwolken abgeleiteten werden. Die Genauigkeit der aus TLS-Punktwolken mit geometrischen Methoden geschätzten Blattfläche kann durch Anwendung eines Moving Least Squares Filters verbessert werden, wodurch Messrauschen und Bewegungseffekte reduziert werden. Diese Forschungsarbeit zeigt, wie mit Hilfe des virtuellen Laserscannings systematisch Variablen untersucht werden können, die die resultierenden Laserscanning-Punktwolken beeinflussen. Indem wir Bäume als dynamische 3D-Objekte modellieren, machen wir zudem einen Schritt hin zu realistischeren simulierten Punktwolken, was virtuelles Laserscanning zu einer leistungsstarken Methode für die Entwicklung von Algorithmen zur Analyse von 4D-Vegetationszeitreihen macht.

Contents

List of Figures

List of Tables

1 Introduction

In ecology, forestry, and precision agriculture, close-range laser scanning has shown great potential for assessing plant health and productivity by deriving proxy variables such as leaf area index (Fang et al., 2019). From the detailed 3D structure that can be obtained using terrestrial laser scanning (TLS), it is also possible to estimate tree volume and ultimately biomass (Disney et al., 2018). Recent work has focused on the movement and change of vegetation. Time series have been acquired to study long-term growth dynamics, regular diurnal or seasonal movement patterns of trees (Calders et al., 2023; Campos et al., 2020; Puttonen et al., 2016; Puttonen et al., 2019; Zlinszky et al., 2017), and response to stress (Jacobs et al., 2021). Wang et al. (2022) developed an open-source software tool for automatic quantification of 3D motion fields of plant structural movements based on TLS point clouds. The tool helps to understand plant dynamics, such as circadian rhythms, growth patterns or wind effects. Circadian movements have been investigated with TLS time series by Puttonen et al. (2016), Puttonen et al. (2019), and Zlinszky et al. (2017). Kattenborn et al. (2022) used deep learning on image time series to predict the temporal variation of leaf angle distributions and validated their method with leaf angle estimates obtained with TLS.

A common problem in these laser scanning applications is the movement of vegetation during the scanning process. TLS requires multiple acquisitions from different positions to completely capture the vegetation and to minimise occlusion. As a result, there is a temporal offset between the acquisitions. The different scans are later co-registered and combined into a single point cloud. However, in almost every outdoor scenario there is wind, which causes leaves and branches to move. Consequently, parts of the vegetation change their position and orientation during and between the scans (Béland et al., 2014). In the combined point cloud, this can result in multiple representations of individual leaves, 'ghosting effects' (Wilkes et al., 2017), blurred leaves or branches, or enlarged branch or stem radii (Vaaja et al., 2016). Seidel et al. (2012) observed reduced canopy openness due to wind-induced branch movement during TLS acquisitions. When analysing multitemporal data, these wind-effects may complicate the differentiation between change related to plant health or growth and regular wind-induced vegetation movement, especially when comparing epochs acquired under different wind conditions.

Although the problem is well known (Disney, 2019; Kükenbrink et al., 2017; Liang et al., 2016; Seidel et al., 2012), few studies systematically investigated the effect of vegetation movement during the scanning process on the derived tree parameters (Demol et al., 2022; Vaaja et al., 2016), or proposed solutions like adapted and more robust algorithms. In terms of TLS data acquisition, it is recommended to scan in weather conditions with low wind speeds, i.e., close to zero (Disney, 2019) or at least below 5 $m\,s^{-1}$ (Seidel et al., 2012). In terms of data pre-processing, Yun et al. (2016) used moving least squares surface approximation (Ridel et al., 2015) to remove the point deviations caused by leaves moving in the wind.

For controlled investigations of wind effects, wind strain may be simulated. Zhang et al. (2022) conducted experiments with a large fan to simulate hurricane-like wind disturbances and investigated the effects on point cloud-derived measures such as leaf angles, effective leaf area index (LAI) or crown volume. To study a large number and variety of trees and different motion magnitudes, it may be preferable to work in a fully virtual environment. Jackson et al. (2019) simulated tree dynamics under windy conditions on quantitative structure models (QSMs) using finite-element analysis. Motivated by this work, Åkerblom and Kaitaniemi (2021) suggest using such tree motion simulations to assign uncertainty values to point clouds acquired under windy conditions in order to remove or correct uncertain points.

Such motion correction, whether directly in the point cloud domain, or later in derived metrics, requires a better understanding of the effects of wind-induced vegetation movement on point clouds and their relationship to acquisition settings and platforms. Virtual laser scanning (VLS) in combination with synthetic dynamic trees is an ideal tool for such systematic investigations, because, in contrast to real surveys, the actual leaf movement is known and wind effects can be distinguished from co-registration errors (or these errors can be neglected). In addition, many different acquisition settings and motion magnitudes can be investigated and compared with low effort (Winiwarter et al., 2022b).

One of the most common applications of VLS in vegetation studies is for testing and validating new point cloud algorithms (Lecigne et al., 2021; J. Liu et al., 2019; Stovall et al., 2021; Vicari et al., 2019; Wang, 2020; Wang et al., 2022; Wu et al., 2021; Zhu et al., 2020) or point cloud metrics (X. Liu et al., 2022). In most of these methodological studies, researchers first present a proof of concept using simulated data before advancing to real use cases. Simulated laser scanning data has the advantage that perfect reference is available in the form of the objects that make up the virtual scene and no manual labelling or manual measurements are required (Winiwarter et al., 2022b).

In this thesis, we simulate terrestrial laser scanning (TLS) and UAV-borne laser scanning (ULS) of dynamic scenes with the VLS software HELIOS++ (Heidelberg LiDAR Operations Simulator) (Winiwarter et al., 2022b) to study the effects of leaf motion. Tadrist et al. (2018) identify two regimes of foliage motion under wind: a) leaf flutter, where leaves move relative to the branches and b) branch turbulence buffeting, the elastic response of branches to wind turbulence, where leaves move together with the branches to which they are attached. With a low dependence on wind speed, leaf flutter dominates at low wind speeds, while branch turbulence buffeting responses dominate at high wind speeds (Tadrist et al., 2018). In this study, we focus on low-wind scenarios and limit the animated tree motion in the laser scanning simulations to different levels of leaf flutter. We hypothesise that the movement of these small scale structures is relevant for high resolution TLS, but negligible for coarser resolution ULS applications. We investigate the effect of leaf motion on different metrics, namely height metrics, voxel-based metrics, geometric features and leaf area estimates. We furthermore analyse the performance of the moving least squares (MLS) filter, in combination with statistical outlier removal (SOR), to reduce motion effects in the TLS point clouds.

In this thesis, the following research questions are addressed:

1. How do moving leaves affect the geometric representation of point clouds acquired by terrestrial and UAV-based laser scanning and how do these effects translate into derived metrics?
2. How sensitive or robust are different point cloud-derived metrics to leaf motion?
3. To what extent can point cloud filtering methods mitigate the effects of leaf motion?

This research contributes to a better understanding of the effects of wind-induced vegetation movement during laser scanning acquisition. It furthermore demonstrates how virtual laser scanning (VLS) can be used to investigate the influence of vegetation movement on commonly used point cloud metrics. This is also one of the first studies employing VLS of dynamic scenes, especially for vegetation point clouds (cf. Winiwarter et al., 2022a for VLS of dynamic topographic scenes).

2 Data and Methods

To study the effects of vegetation movement, we create three scenarios of leaf flutter and one static scenario for 15 small computer-generated trees. Multi-scan terrestrial laser scanning (TLS) and UAV-borne laser scanning (ULS) simulations are carried out for each tree and scenario in HELIOS++[1] (Winiwarter et al., 2022b). HELIOS++ is an open-source, general-purpose virtual laser scanning software that supports scenes with dynamic objects, i.e., objects that experience rigid motion during the simulation. Using various point cloud-derived metrics, we explore the differences between the movement scenarios. Furthermore, using both a real TLS point cloud and the simulated TLS point clouds, we investigate the effect of point cloud filtering on the metrics, namely the moving least squares (MLS) filter in combination with statistical outlier removal (SOR). The entire workflow is presented in Figure 1. This chapter explains the methods, from the generation of synthetic trees and the animation of leaf motion, to laser scanning simulations and metric calculations.

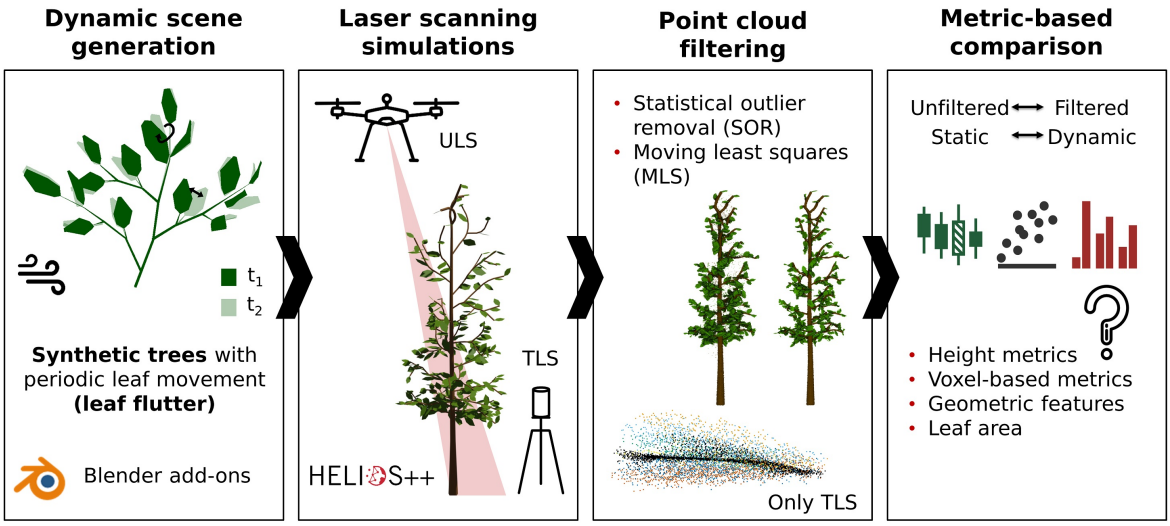

Figure 1: Schematic workflow of the study. TLS = Terrestrial laser scanning, ULS = UAV-borne laser scanning. Icon "wind" in the left panel made by Freepik from www.flaticon.com, icons "candlestick chart", "scatter chart", and "grouped bar chart" in the right panel from loading.io.

[1]https://github.com/3dgeo-heidelberg/helios

2.1 Data

2.1.1 Synthetic trees

Laser scanning simulations require a 3D model of the object or phenomenon of interest. In this study, these are synthetic tree models with leaves, to which rigid motions (more specifically, rotations) are applied to simulate wind-induced leaf flutter.

The models have to fulfil a number of requirements:

1. Trees must be three-dimensional.
2. Trees must have an appropriate level of resolution and quality.
3. Trees must have leaves (leaf-on canopy condition).
4. Each moving part, i.e., each leaf, must be a separate object.
5. Each leaf must be attached to the stem at a single point (here called the leaf base), which also serves as the centre of rotation of the leaf in the leaf motion model.
6. It must be possible to save the tree geometry as triangle mesh in a format compatible with HELIOS++, i.e., Alias/Wavefront OBJ geometry format.

In order to parameterise a dynamic tree model from real high-resolution laser scanning data or from tree images, it should furthermore be possible to

7.a generate the trees based on parameters observable in point clouds or in images or
7.b reconstruct the tree directly and automatically from laser scanning point clouds.

A popular method for creating realistic trees from a set of parameters (Requirement 7.a) is the algorithm presented by Weber and Penn (1995), which is implemented in the software *Arbaro*[2], the Blender add-ons *Sapling Tree Gen*[3] and *tree-gen*[4], the Helios *Weber-Penn Tree Plugin*[5] or the OpenAlea extension *Weberpenn*[6]. The algorithm meets the following criteria (Weber & Penn, 1995):

- Trees are three-dimensional (Requirement 1).
- Trees have an appropriate level of resolution and quality (Requirement 2).
- Trees can have leaves, which are attached to the stem at their leaf base (Requirements 3 and 5).
- A wide variety of tree types and related vegetation (e.g., shrubs, bushes, large grasses) can be created using different parameters and random variations.

[2] https://sourceforge.net/projects/arbaro/
[3] https://docs.blender.org/manual/en/latest/addons/add_curve/sapling.html
[4] https://github.com/friggog/tree-gen
[5] https://baileylab.ucdavis.edu/software/helios/_weber_penn_doc.html
[6] https://openalea.readthedocs.io/en/latest/tutorials/visualea/weberpenn.html

- Parameters are easy to understand for a typical user and do not require an understanding of difficult mathematical principles or knowledge of technical botanical terminology (Requirement 7.a).
- The parameters are able to create the tree geometry efficiently.

The parameters include the shape of the tree (e.g., conical, spherical, cylindrical, flame), the size (height) and scaling of the tree, the levels of recursion, the branching and spiralling angles of the branches, the number of leaves per branch, leaf shape, leaf size and many more. Branching parameters are available for each level (main branches, secondary branches, tertiary branches and so on).

When attempting to create trees of a certain type or species with the Weber and Penn (1995) algorithm, it is recommended to use images or 3D point clouds of the tree as a template. Some parameters can be directly measured from the tree (e.g., tree height), others can be tweaked by experimentation and visual comparison. In Blender (version 3.4, Blender Online Community, 2022), which we used in this work, the resulting 3D tree models consist of the woody structure, which is a 'curve' object, and the entirety of the leaves, which is a mesh object. Trees generated with *tree-gen* can furthermore have flowers. In a post-processing step in Blender, the stem curve is transformed into a mesh and the leaves are separated 'by loose parts', i.e., every disconnected fragment is a separate leaf object (Requirement 4). In this way, the objects that make up a tree can be exported from Blender in various formats, including Alias/Wavefront OBJ (Requirement 6).

A further approach is modelling trees directly from a TLS point cloud (Requirement 7.b) by reconstructing branch topology (Côté et al., 2009; D.-M. Yan et al., 2009) and fitting cylinders (Raumonen et al., 2013). Such models are referred to as quantitative structure models (QSMs). There are different algorithms for QSM generation. Two of the most widely used implementations are *TreeQSM* (Raumonen & Åkerblom, 2022; Raumonen et al., 2013) and the *SimpleForest* (Hackenberg, 2021; Hackenberg et al., 2014) plugin for Computree (Computree group, 2020).

In this thesis, ten synthetic apple trees are created using procedural modelling with the Blender add-on *Sapling Tree Gen* and five synthetic apple trees, with flowers, are created with the Blender add-on *tree-gen*. As a visual template, real TLS apple tree point clouds are used (Section 2.1.2). The 15 virtual trees are similar in their general dimension but differ in terms of the number, distribution, and size of branches and leaves. The trees are between 2.47 m and 2.98 m tall, have between 88 and 387 leaves and a total leaf area between 0.44 m^2 and 1.54 m^2. Figure 2 shows the 15 simulated TLS apple tree point clouds (without movement) and the real TLS apple tree point cloud serving as reference.

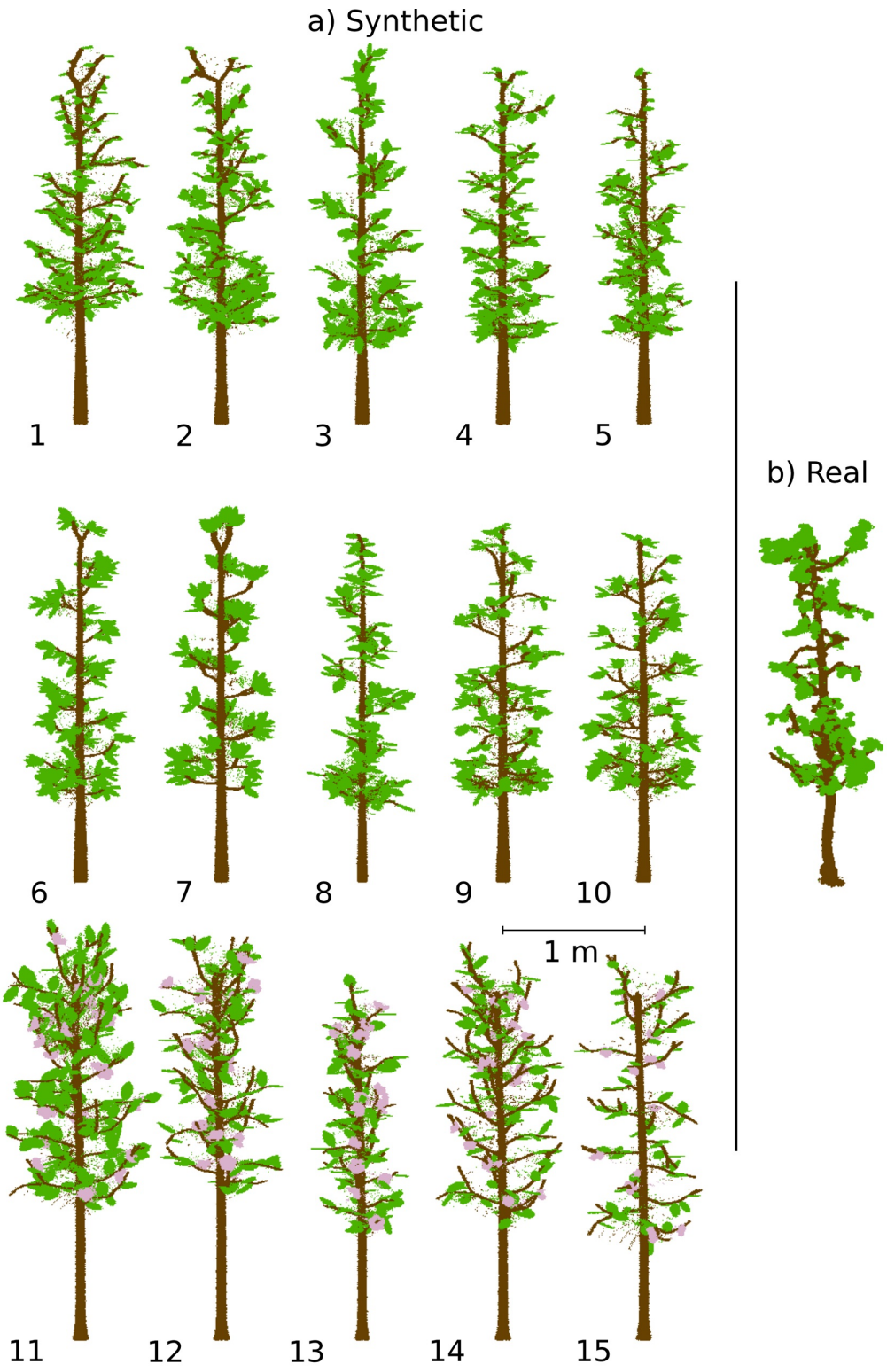

Figure 2: a) Simulated terrestrial laser scanning (TLS) point clouds (without leaf motion) of the 15 synthetic trees and b) real TLS tree point cloud, all coloured by classification (brown = wood, green = leaf, pale pink = flower). The top two rows show trees generated with *Sapling Tree Gen* and the bottom row shows the trees generated with *tree-gen*.

2.1.2 Real-world laser scanning point cloud

A real terrestrial laser scanning (TLS) point cloud of an apple tree is used as a template for the creation of synthetic trees. In addition, the effects of the point cloud filtering approach are investigated not only on the simulated point clouds, but also on the real point cloud.

Data were collected in collaboration with the Precision Horticulture research group at the Leibniz Institute for Agricultural Engineering and Bioeconomy (ATB) in an apple orchard in Potsdam-Marquardt, Germany (52.4660° N, 12.9579° E), which is part of ATB's Fieldlab for Digital Agriculture. Ten trees standing in an orchard row were scanned with a *RIEGL* VZ-2000i terrestrial laser scanner (RIEGL LMS, 2022a) on 11 May 2022 from 12 scan positions (SPs) under moderately windy conditions. The horizontal and vertical angular resolution was 0.007° and the pulse repetition frequency was 1200 kHz. Six reflective targets were placed in the scene to support the co-registration of scans. At two positions (SP1 and SP8) on each side of the orchard, two scans were performed consecutively, to capture motion differences from the same position. Furthermore, at two positions on either side of the orchard (SP9 and SP12), the tripod was set to minimum height to increase the variety of different viewing angles on the trees.

For pre-processing and co-registration, the single scans are imported into RiSCAN PRO, version 2.12.1, the Operating & Processing Software for 3D Laser Scanners by RIEGL LMS (2022b). Points with a *RIEGL* reflectance below −25.0 dB and above 5.0 dB or with a *RIEGL* pulse shape deviation above 25 are deleted from the individual scans. The scans are co-registered using the reflectors as tiepoints, which were visible from multiple positions. Finally, a fine alignment is performed using the multi station adjustment (MSA) in RiSCAN PRO which uses corresponding planar surfaces (plane patches) to minimise the distances between scans. The final MSA error (standard deviation) is 0.0044 m.

One tree is manually extracted from the point cloud and then labelled into wood and leaf points using the 'Interactive Segmentation Tool' of CloudCompare (CloudCompare, 2022). Before further processing (moving least squares filtering and estimation of metrics), the tree point cloud is cleaned with the statistical outlier removal (SOR) filter (with knn=6 and m=1.0, cf. Section 2.4) and subsampled with Poisson sampling with a minimum distance between points of 0.0025 m using PDAL (PDAL Contributors, 2022).

2.2 Animated motion

To animate leaf flutter, we developed an add-on for Blender 3.4 (Blender Online Community, 2022) which makes use of the Blender Python API[7]. The *Move Leaves* add-on is part of the GitHub repository *movingtree_b2h*[8]. It operates on a scene with a single tree as generated by, e.g., the *Sapling Tree Gen* add-on or the *tree-gen* add-on with one mesh object containing the woody components and many more mesh objects for the individual leaves. Different parameters allow the configuration of the duration of the scene (here always 120 frames), the fraction of moving leaves and the magnitude of the motions. A leaf angle distribution can also be specified, which is applied before the animation is generated, as this distribution is not available as a parameter in the Weber and Penn algorithm.

Light (a), moderate (b) and heavy (c) leaf motion scenarios are predefined as specified in Table 1. As orientation for these scenarios, we used the observations by Bschorr (1991) and Tadrist et al. (2018). In the animation, the leaves of the tree rotate (oscillate) around the leaf base at regular intervals. The duration of these intervals in number of frames is determined be the animation frame rate (here 24 fps) and the oscillation frequency. In each interval, Euler angles are sampled from normal distributions according to Table 1, a global XYZ-Euler rotation is defined from these angles and applied to the leaf, and an animation keyframe is inserted. Blender then interpolates between the keyframes to create a smooth transition between the different leaf orientations. Although each leaf moves differently, the rhythm of the movement is synchronised, i.e., the times at which the keyframes are inserted are the same.

Table 1: Parameters of the three leaf motion scenarios. For each oscillation, the Euler rotations are determined by sampling from the specified normal distributions with the X-angle being the largest component of the rotation.

	static	a	b	c
Leaf angle distribution	planophile	planophile	planophile	planophile
Fraction of leaves moving	0.0	0.5	1.0	1.0
Frequency	-	6 Hz	6 Hz	6 Hz
X-angle $\sim N(\mu, \sigma^2)$	-	$\mu = 0°, \sigma = 8°$	$\mu = 0°, \sigma = 8°$	$\mu = 0°, \sigma = 16°$
Y-angle $\sim N(\mu, \sigma^2)$	-	$\mu = 0°, \sigma = 2°$	$\mu = 0°, \sigma = 2°$	$\mu = 0°, \sigma = 4°$
Z-angle $\sim N(\mu, \sigma^2)$	-	$\mu = 0°, \sigma = 2°$	$\mu = 0°, \sigma = 2°$	$\mu = 0°, \sigma = 4°$

[7] https://docs.blender.org/api/current/index.html
[8] https://github.com/han16nah/movingtree_b2h

2.3 Laser scanning simulation

Animated scenes are converted into HELIOS++ compatible formats and then scanned virtually in two platform modes: Static terrestrial laser scanning (TLS) and UAV-borne laser scanning (ULS). Each virtual scene contains a single synthetic tree whose stem base is centred at the origin position $O(0, 0, 0)$. The simulated point clouds of the individual scan positions or flight strips are merged into one compressed LAS point cloud file (LAZ) and the scan position IDs or flight line IDs are stored in the LAZ field point source ID.

2.3.1 Scene configuration

The tree scenes animated in Blender are exported to a HELIOS++ XML scene file with rigid motions using the specially developed add-on `movingtree_b2h`. In each loop over the keyframes, the rotation between the previous and the current rotation is determined for each leaf and converted to an axis-angle-representation, creating a sequence of rotations for each leaf. After the last sequence (i.e., the last keyframe), the motion starts again with the first rotation sequence, forming an infinite loop. The leaf base is used as the rotation centre, so that the leaf base always remains in the same location. To control the speed of the rigid motions, the parameter `dynStep` is used, which defines the frequency of a dynamic scene step relative to the operating frequency of the simulation (which is equal to the pulse frequency of the scanner). In our work, a frequency of 12 500 is used, which for a pulse frequency of 300 000 Hz gives a virtual time per dynamic operation of $1/300\,000\,\text{s} \cdot 12\,500 = 0.041\,67\,\text{s}$. With that, each dynamic time step in HELIOS++ has the same duration as one frame in Blender, i.e., 1 divided by the frame rate, in our case $1/24\,\text{fps} = 0.041\,67\,\text{s}$. We also set the `kdtDynStep` to 100, which means that the HELIOS++ data structure that handles multiple KDTrees for efficient ray casting on dynamic scenes, the KDGrove, is updated after 100 object updates, i.e., every 4.167 s.

Besides the light, moderate and heavy leaf motion scenarios (Table 1), a static scene without any motion is generated for each tree. The XML file of this scene contains only the scene parts (stem, leaves, possibly flower) without any rigid motions.

Some later processing steps (e.g., point cloud filtering, metric estimation) are only performed on leaf points and not on wood points. Therefore, the simulated point clouds have to be labelled as leaf, wood, and possibly blossom (Figure 2). This is done by setting a `helios_classification` parameter in the material definitions stored in the material files (.mtl) associated with the objects in the OBJ files. The object's classification value is then automatically assigned to all returns which are generated on the object's surface. We defined the three materials: 'trunk and branches' (classification = 0), 'leaves' (classification = 1), and 'blossom' (classification = 2).

2.3.2 Virtual terrestrial laser scanning (TLS)

Terrestrial laser scanning simulations are conducted from six scan positions regularly distributed around each tree in a circle of 3 m radius (Figure 3a). A virtual laser scanner of the model *RIEGL* VZ-400 (RIEGL LMS, 2017) is used with the scan settings reported in Table 2. The vertical and horizontal resolution of 0.04° results in a point spacing of 0.7 cm in 10 m range, or 0.21 cm in 3 m range in the single scans. The scanner is mounted at a tripod height of 1.5 m with an additional vertical offset of 0.2 m for the scanner, resulting in the beam origin at 1.7 m height.

Table 2: Scan settings used for each of the six scan positions in the terrestrial laser scanning simulations.

Scanner	*RIEGL* VZ-400
Horizontal resolution	0.04°
Vertical resolution	0.04°
Pulse repetition frequency	300 kHz
Beam divergence	0.27 mrad @ $1/e^2$
Accuracy	0.005 m

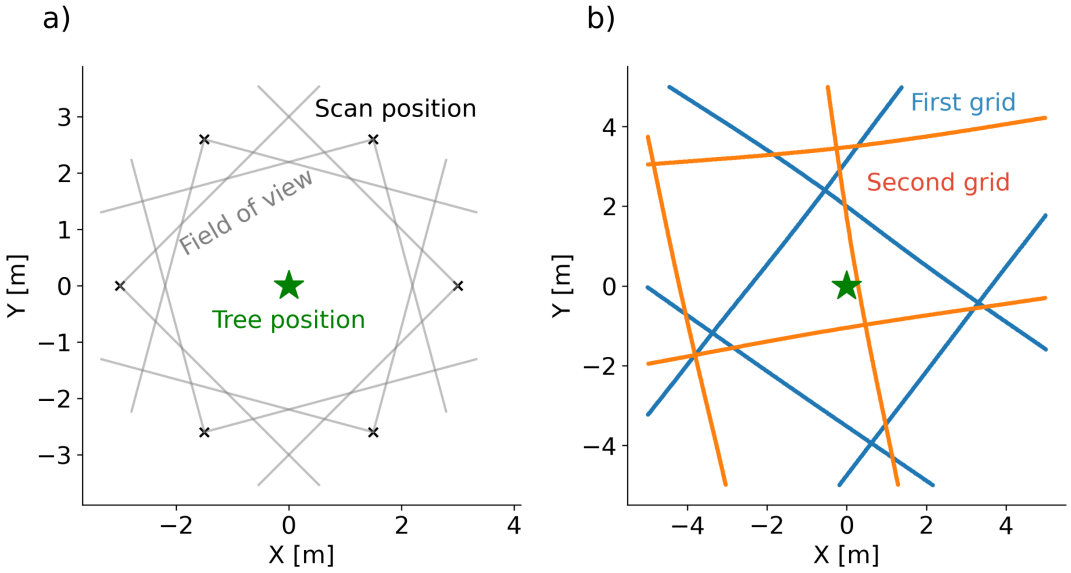

Figure 3: Survey plans of a) the terrestrial laser scanning (TLS) and b) the UAV-borne laser scanning (ULS) simulations. The black crosses mark the TLS scan positions, the grey lines mark the start and the end of the field of views. The ULS flight lines are shown as blue lines (first grid) and orange lines (second grid, rotated by 45° with respect to the first grid). The green star marks the position of the tree.

2.3.3 Virtual UAV-borne laser scanning (ULS)

In the UAV-based laser scanning simulations, eight flight lines are flown over the synthetic trees, arranged in two overlapping grids at a 45° angle to each other (Figure 3b). The flight pattern is specified as a trajectory file with the columns X, Y, Z, Time, Roll, Pitch, Yaw. This trajectory was derived from real acquisitions over the apple orchard of the Fieldlab for Digital Agriculture by ATB and has been translated into a local coordinate system, so that the centre of the flight grid is at the origin $O(0, 0)$, which is also the horizontal position of the synthetic tree. The first grid is at a height of between 14.1 m and 14.9 m, the second grid between 15.6 m and 16.6 m. A virtual laser scanner of the model *RIEGL* VUX-1UAV[22] (RIEGL LMS, 2023) is used with the scan settings specified in Table 3.

Table 3: Scan settings used in the UAV-based laser scanning simulations.

Scanner	*RIEGL* VUX-1UAV[22]
Pulse repetition frequency	300 kHz
Scan frequency	100 Hz
Beam divergence	0.5 mrad @ $1/e^2$
Accuracy	0.01 m

2.4 Point cloud filtering

Point cloud filtering is a typical part of the point cloud processing chain and can significantly improve the quality of the information derived from the point cloud. In the case of (moving) tree point clouds, different filtering techniques can help to remove noise (e.g., 'ghost points' in the air, irregularities due to small distance measurement errors or object motion) from the point cloud.

The statistical outlier removal (SOR) filter (Rusu et al., 2008) removes sparse outliers based on the mean μ and standard deviation σ of the nearest neighbour distances of all points. The user provides a neighbourhood (K-nearest neighbours knn) and a standard deviation multiplier m and the SOR algorithm removes all points for which the mean distances to the knn is above the threshold $T = \mu \pm m \cdot \sigma$. The moving least squares (MLS) filter (Alexa et al., 2003; Levin, 2004; Ridel et al., 2015) has been used by Yun et al. (2016) to mitigate the effect of leaves shaking during acquisition by obtaining a clear single leaf representation from the deviant leaf representations of single scans. MLS approximates the surface with polynomials (Alexa et al., 2003). A comparison of (moving) tree point clouds and single leaf point clouds from TLS before and after MLS filtering is shown in Figure 4.

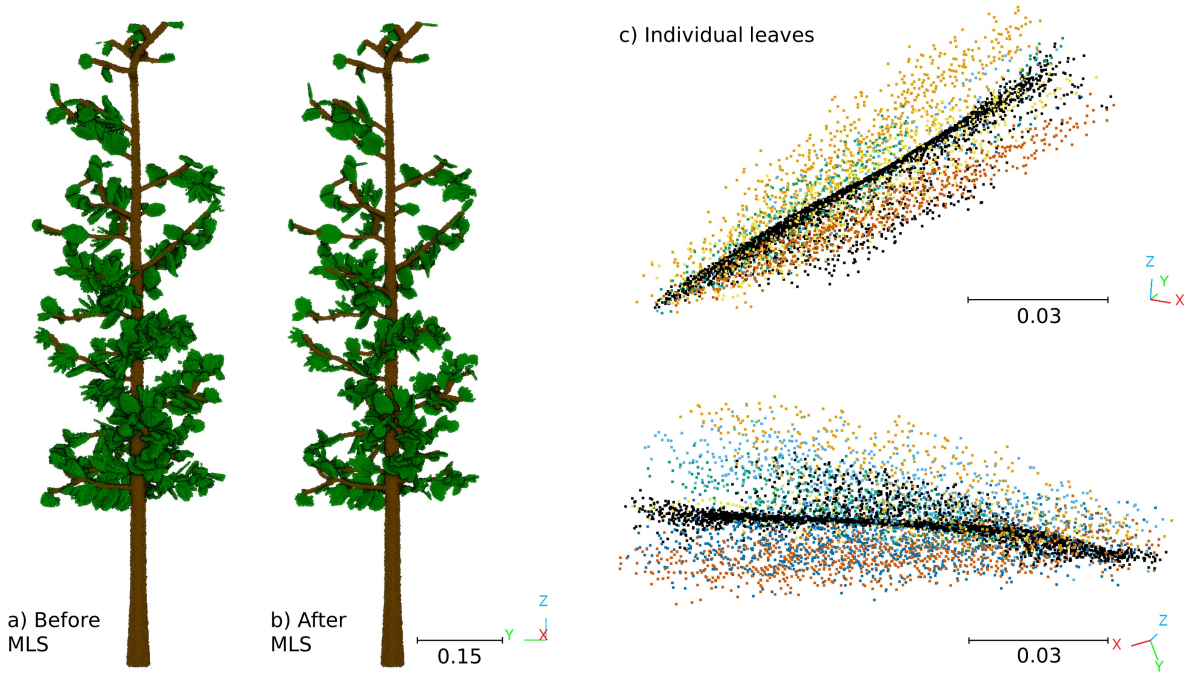

Figure 4: Illustration of the moving least squares (MLS) filter. The left side shows a terrestrial virtual laser scanning tree point cloud in motion scenario c before (a) and after (b) running the MLS filter on the leaf points. The point clouds are coloured by classification (brown = wood, green = leaf). (c) shows point clouds of two individual leaves which were moving during VLS, with the unfiltered points coloured by scan position and the MLS-filtered points in black.

We only apply the filtering procedure to TLS point clouds for the following reasons: a) There are no visible outliers in the ULS point clouds (Figure 15). Due to the lower point density, the SOR filter would likely either remove too many or barely any points. b) The MLS filter is used to smooth and resample points from the leaf surfaces to get a better representation of leaves. In ULS point clouds, too few points are available per leaf (usually less than 10) to approximate the leaf surfaces.

To investigate how the two filters improve or deteriorate the metrics estimated from the TLS data, we apply the SOR filter on the tree point clouds followed by the MLS surface approximation on just the leaf points. The settings for the two algorithms are reported in Table 4 for both the simulated point clouds and the real point cloud.

Table 4: Settings for the statistical outlier removal (SOR) and the moving least squares (MLS) filter applied to the terrestrial laser scanning (TLS) point clouds.

Setting	Value
Statistical outlier removal (SOR)	
K-nearest neighbours knn	6
Standard deviation multiplier m	1.0
Moving least squares (MLS) filter (simulated data)	
Search radius r	0.05 m
Polynomial order	1
Moving least squares (MLS) filter (real data)	
Search radius r	0.1 m
Polynomial order	1

2.5 Calculation of Metrics

We explore the effects of leaf motion on the individual trees using several metrics listed in Table 6. Height metrics and voxel-based metrics are computed for both TLS and ULS point clouds, geometric features and leaf area are only derived for TLS point clouds. In the TLS case, the metrics are calculated from both the unfiltered and the filtered point clouds.

2.5.1 Height metrics

The first category of metrics are height metrics. They describe the vertical distribution of points and relate to the tree or forest structure. Height metrics are a standard, particularly in airborne laser scanning (ALS)-based forest inventories, to estimate plot-based characteristics based on the correlation of the laser scanning height metrics and forest inventory attributes.

2.5.2 Voxel metrics

The second group of metrics encompasses voxel-based metrics, namely the percentage of filled voxels, which allows quantifying gaps in the tree crowns, and the number of points per voxel, which can give an estimate of the clumping of points. We perform voxelization for three voxel sizes, 0.02 m, 0.05 m, and 0.1 m for the TLS point clouds and 0.05 m, 0.1 m and 0.25 m for the ULS point clouds. For the TLS voxelization, we discard voxels with less than 3 points per voxel, for the ULS voxelization, no points are discarded.

2.5.3 Geometric features

The third set of metrics are geometric features, which are computed for each point based on its local neighbourhood. We select the dimensionality features (or shape features) linearity L_{λ_3D}, planarity P_{λ_3D}, and sphericity (also called scattering) S_{λ_3D} (Weinmann et al., 2015). Furthermore, we include verticality V_{λ_3D}, which is computed from the vertical component of the local normal vector (Weinmann et al., 2015). One of the main applications of these geometric descriptors is as features for machine learning-based semantic segmentation of point clouds, such as leaf-wood classification (Wang et al., 2017; Xi et al., 2020; J. Zhou et al., 2019).

2.5.4 Leaf area

The last metric, leaf area (LA), is particularly relevant in ecological, forestry, and agricultural research and practice. A variety of essential energy, water and gas exchange processes take place in plant leaves, such as photosynthesis, transpiration, respiration and nutrient uptake. In 1947, the leaf area index (LAI) was introduced by D. J. Watson (1947) for comparing agricultural yields and is defined as the total one-sided leaf area per horizontal unit ground area [m^2/m^2]. LAI has proven to be an important variable for vegetation structure (Running & Coughlan, 1988) and has been listed as essential climate variable by the UNFCCC (Mason et al., 2003). In the priority list of biodiversity metrics to observe from space (Skidmore et al., 2021), LAI is one of the highest ranked metrics and occurs in multiple essential biodiversity variable classes (ecosystem physiology, habitat structure and species physiology). As LAI is related to the amount of light absorbed by the canopy, it can be used to estimate photosynthesis rates, primary productivity and biomass production. For example, LAI has been used by Running and Coughlan (1988) as an independent variable for calculating transpiration, respiration, photosynthesis and carbon flux in their model to estimate primary production. In agriculture and horticulture, LAI is an essential parameter to assess plant growth and health status, to study the effects of management practices, or to predict yield (Fang et al., 2019; Heuvelink et al., 2005; Kalisperakis et al., 2015; Strachan et al., 2005).

There are several ways to estimate LA from TLS and ULS data (G. Yan et al., 2019). Due to the high spatial resolution and point density, LA can be measured directly from TLS point clouds using geometric methods (Boukhana et al., 2022). We applied three methods for direct LA estimation from TLS point clouds.

First, similar to Yun et al. (2016) and Yun et al. (2019), we use 2.5D Delaunay triangulation of leaf points to obtain LA. For this approach, we first filter all input point clouds (i.e., also the 'unfiltered' one) with the SOR algorithm with the settings reported in Table 4 (knn = 6, m=1.0). Leaves are then separated, which for the simulated point clouds can be done by the HELIOS++ parameter 'Object ID'. However, this and other point cloud attributes are lost during MLS smoothing. Therefore, in the real point cloud and in all filtered point clouds (simulated, real), the leaves are separated by region growing segmentation. Region growing segmentation aims at grouping points belonging to smooth surface patches (Rabbani et al., 2006). The algorithm starts with normal estimation followed by curvature approximation using the residuals of local plane fitting. Based on a local connectivity constraint (using only neighbouring points during region growing) and a surface smoothness constraint (angle between normals, curvature threshold), points are then segmented (Rabbani et al., 2006). The constraints are controlled by user-specified parameters. The parameter settings used in this work to segment the leaves in the simulated point clouds and the real point cloud are reported in Table 5.

Each leaf point cloud is subsampled with a minimum distance between points of 0.004 m and then projected onto the best fitting plane (obtained by least squares) before a 2D triangulation is computed and the resulting mesh structure is applied to the 3D points[9]. A maximum edge

[9] https://www.cloudcompare.org/doc/wiki/index.php/Mesh%5CDelaunay_2.5D_(best_fit_plane)

Table 5: Settings for the region growing segmentation applied to the simulated and real terrestrial laser scanning point clouds. MLS = Moving least squares.

Setting	Value	
	Simulated point clouds	**Real point cloud**
Search radius (for normal computation)	0.1 m	0.1 m
Minimum cluster size	10 points	10 points
Maximum cluster size	150 000 points	1 000 000 points
K-nearest neighbours *knn*	50 points	50 points
Smooth threshold	2°	5° (before MLS filter) 2° (after MLS filter)
Curvature threshold	1	2
Residual threshold	1	1

length of 0.04 m is set to remove long edges in the void in occluded regions or gaps between (incorrectly segmented) leaves (Yun et al., 2016). LA_{tri} is then obtained by summing the areas of the remaining triangles.

Second, we adopt the envelope fitting method by You et al. (2022) and use the alpha shape algorithm (Edelsbrunner & Mücke, 1992) on the leaf point cloud to obtain the leaf envelopes. For this, we use the alpha shape implementation in Open3D (Q.-Y. Zhou et al., 2018) and an alpha value of $\alpha = 0.015$. Because 3D alpha shapes are volumes and not surfaces, the total one-sided leaf area LA_{α} is calculated as half of the surface area of the canopy alpha shape.

Third, LA is estimated using screened Poisson surface reconstruction (Kazhdan et al., 2006), as implemented in Open3D. Since Poisson surface reconstruction works on oriented point sets, we first perform normal estimation with a search radius of 0.05 m. The Poisson surface reconstruction algorithm reconstructs a single closed surface from the point cloud of all the leaves (as opposed to separate surfaces for each leaf), but also outputs a density value per triangle. Triangles with low density values are only supported by a small number of points and can therefore be removed in our application. As recommended by Boukhana et al. (2022), we trim the mesh by removing all triangles with a density lower than the mean density of all triangles. Again, $LA_{poisson}$ is calculated by summing the areas of all the remaining triangles.

For the alpha shapes and the Poisson surface reconstruction, leaves do not have to be separated in the input point clouds. Figure 5 illustrates the three geometric methods for direct leaf area (LA) retrieval from TLS point clouds on a point cloud subset.

Another method of obtaining LA is to estimate the leaf area density (LAD; leaf area per unit volume [m^2/m^3]) per voxel, based on the attenuation of light by canopies. In the case of laser scanning, light attenuation or canopy transmittance can be derived from the ratio of traversing laser pulses to entering laser pulses (Béland et al., 2014; Pimont et al., 2018; Vincent et al., 2017;

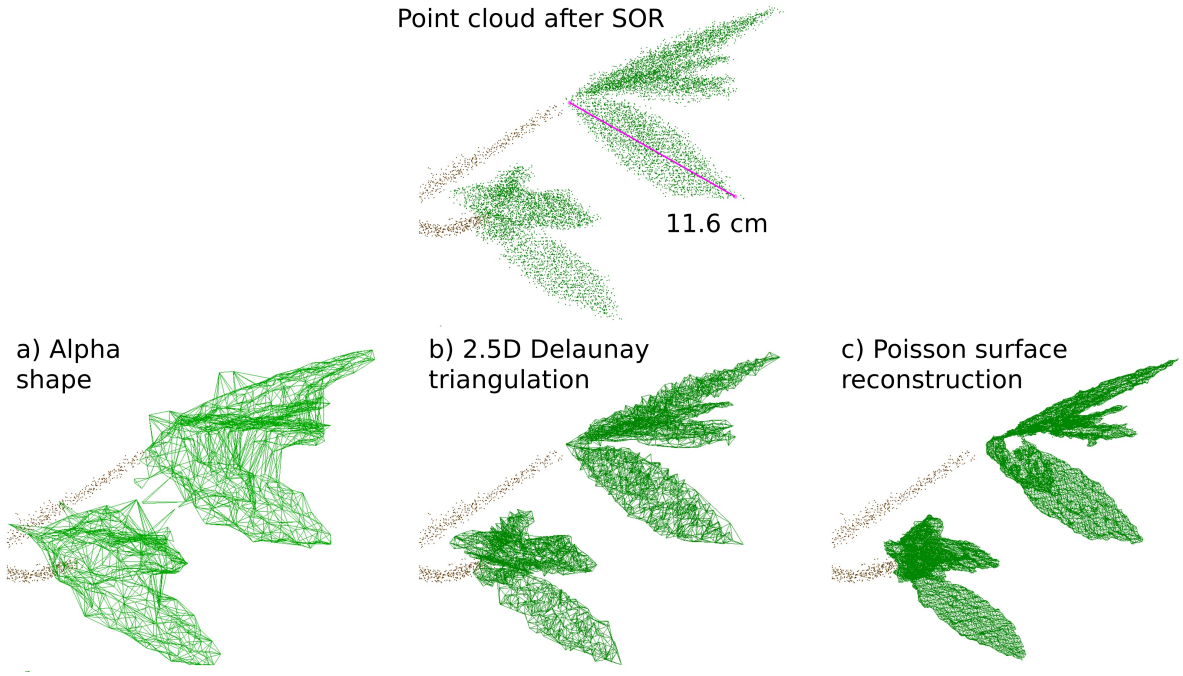

Figure 5: Comparison of the three geometric methods for direct leaf area retrieval from terrestrial laser scanning point clouds. The top image shows a point cloud of a branch and multiple leaves, simulated in the static scenario after statistical outlier removal (SOR). The bottom images show the triangle meshes obtained with the tree methods: a) Alpha shape b) 2.5D Delaunay triangulation (per leaf), and c) Poisson surface reconstruction. While the alpha shape results in a volume, and leaf area is therefore obtained as half of the mesh surface area, the Delaunay triangulation and the Poisson surface reconstruction result in a surface.

G. Yan et al., 2019). This approach is also suitable for ULS scans, where individual leaves are not sampled well enough to apply the geometric methods. We used the software AMAPVox[10] for light transmittance/attenuation-based leaf area estimation (Vincent et al., 2017). In addition to the simulated point cloud in LAS/LAZ format, the positions of the sensor at each time step must be provided. For the ULS case, we specified the ASCII files with the trajectory points, which contain a (virtual) GPS time attribute corresponding to the GPS time attribute in the point cloud. For the TLS case, we specified the scanner position for each scan. With these inputs, AMAPVox performs ray tracing from the scanner head to the recorded hit through a voxel grid to derive the leaf area density, taking into account sensor parameters (laser beam footprint and beam divergence, which determine the theoretical beam fraction at a given distance) and canopy parameters (leaf angle distribution and mean leaf area). In a first step, the effective sampling area of each laser pulse (or laser pulse fraction in case of multiple hits) is calculated from the theoretical beam cross-section and the remaining beam fraction entering a voxel. The sampling area is then combined with the optical path length of the pulse entering the voxel to compute the local transmittance or local attenuation (Vincent et al., 2021). We used cubic voxels and a voxel size of 0.1 m and filtered the input tree point cloud by classification to use only leaf points for the estimation. We also defined the sensor parameters for the *RIEGL* VUX-1UAV[22] (ULS) and

[10]https://amapvox.org/

the *RIEGL* VZ-400 (TLS) and a planophile leaf angle distribution (Section 2.2). Total leaf area is calculated from voxel-based LAD estimates by summing all LAD values and multiplying by the voxel volume. For each of our motion scenarios, we compare the different LAD estimation procedures implemented in AMAPVox and described by Vincent et al. (2021):

1. Transmittance (or also gap probability) estimation
2. Attenuation estimation (Maximum likelihood estimators; MLE)
    2.a Potential path length (PPL) estimator
    2.b Free path length (FPL) estimator

For the FPL estimator, a bias correction is included which considers the cross-sectional area of a single vegetation element (Vincent et al., 2021). For this bias correction, we provided the exact mean leaf area for each tree, as estimated from the input tree models.

Table 6: Overview of the metrics that have been investigated for their sensitivity to animated leaf motion. $EV1$, $EV2$, $EV3$ = Eigenvalues, such that $EV1 \geq EV2 \geq EV3$, NV_z = vertical component of the normal vector, TLS = Terrestrial laser scanning, ULS = UAV-borne laser scanning.

Metric	Description	Category
$\mathbf{H}_{mean}$	Mean height [m]	Height metrics
$\mathbf{H}_{sd}$	Standard deviation of height [m]	
$\mathbf{D}_{\{10,20,...,90\}}$	Height deciles [m]	
$\mathbf{\%Vox}_{filled}$	Percentage of filled voxels for voxel sizes a) TLS: 0.02 m, 0.05 m and 0.1 m (threshold: 3 points per voxel) b) ULS: 0.05 m, 0.1 m and 0.25 m	Voxel-based features
$\mathbf{PPVox}_{median}$	Median number of points per voxel	
$\mathbf{PPVox}_{max}$	Maximum number of points per voxel	
$\mathbf{PPVox}_{sd}$	Standard deviation of number of points per voxel	
Linearity $\mathbf{L}_{\lambda\_3D}$	Linear saliency $(EV_1 - EV_2)/EV_1$ [m]	Geometric features (TLS)
Planarity $\mathbf{P}_{\lambda\_3D}$	Planar saliency $(EV_2 - EV_3)/EV_1$ [m]	
Sphericity $\mathbf{S}_{\lambda\_3D}$	Volumetric saliency EV_3/EV_1 [m]	
Verticality $\mathbf{V}_{\lambda\_3D}$	$1 - NV_z$ [m]	
$\mathbf{LA}_{\alpha}$	Leaf area [m^2] - 3D alpha shapes	Leaf area (TLS) (direct geometric methods)
$\mathbf{LA}_{tri}$	Leaf area [m^2] - 2.5D Delaunay triangulation	
$\mathbf{LA}_{poisson}$	Leaf area [m^2] - screened Poisson surface reconstruction	
$\mathbf{LA}_{t}$	Leaf area [m^2] - from voxel-based light transmittance	Leaf area (indirect methods)
$\mathbf{LA}_{att\_ppl}$	Leaf area [m^2] - from voxel-based light attenuation using the potential path length (PPL) estimator	
$\mathbf{LA}_{att\_fpl}$	Leaf area [m^2] - from voxel-based light attenuation using the free path (FPL) length estimator	

3 Results

The aim of this research is to investigate how vegetation movement during acquisition affects the different metrics presented in Section 2.5 and how these effects are modified by point cloud filtering. In this chapter, we present the results of the metric-based comparisons, first for the simulated TLS point clouds, before filtering and after filtering, and then for the ULS point clouds.

3.1 Metrics derived from terrestrial laser scanning (TLS) point clouds

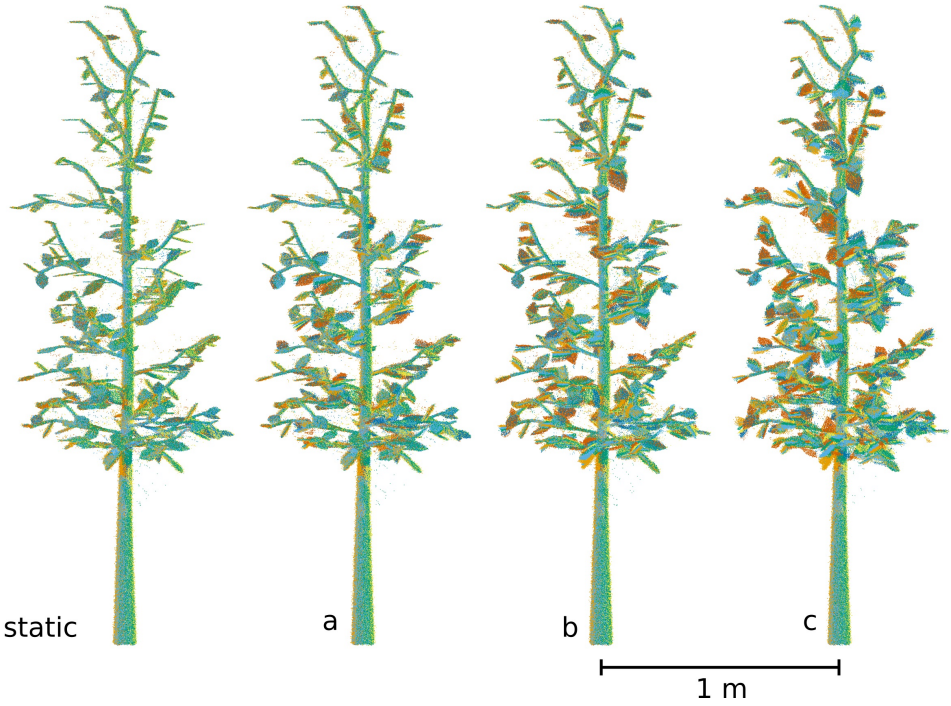

Figure 6: Comparison of terrestrial laser scanning tree point clouds for tree 1 simulated in the four different motion scenarios, coloured by point source ID (i.e., scan position).

The simulated TLS point clouds of one synthetic tree (tree 1) are shown in Figure 6 for all motion scenarios. Before looking at the calculated metrics, the total number of points and the number of points per class (leaf, wood) are compared. The simulated TLS point clouds have between 410 000 and 990 000 points. The mean number of points, averaged over all 15 trees, varies from 543 300 (static scenario) to 587 000 (scenario c). With an average of about 70%, the majority of the points are leaf points (including blossom points). With more leaf movement, the number of leaf points increases (by about 47 250 points on average from static to c) and the

number of wood points decreases (by about 3500 on average from static to c), so that the total number of points increases by about 43 750 (8%) on average from static to c.

Filtering reduces the average number of points by about 30 000 to 40 000: 29 000 points (5 %) in the static scenario and 40 250 (7 %) in scenario c. This reduction is mainly due to the SOR filter, which removes points from the point cloud. The MLS smoothing changes the positions of the points by resampling but does not change the number of points notably.

3.1.1 Height metrics

There is a slight increase in the mean height H_{mean} from the static scenario to the motion scenario c. In contrast, the standard deviation of height H_{sd} decreases slightly from the static scenario to scenario c (Table 7). However, the differences are only in the order of a few millimetres. Filtering with the SOR filter and the MLS filter does not influence H_{mean} or H_{sd}.

Table 7: Mean height H_{mean} and standard deviation of height H_{sd} of simulated terrestrial laser scanning point clouds averaged over all trees (N=15) by motion scenario.

Scenario	H_{mean}	H_{sd}
static	1.391 m	0.603 m
a	1.396 m	0.601 m
b	1.397 m	0.599 m
c	1.406 m	0.595 m

Figure 7 shows the averaged height deciles for the different motion scenarios. The lowest values are observed for the static scenario, the highest values for scenario c. The differences are between 1.4 cm and 2.4 cm for D_{10} to D_{70} and below 1 cm for D_{80} and D_{90}. The values of the height deciles are hardly changed by the point cloud filtering and the differences between unfiltered and filtered point clouds are in the range of a few millimetres.

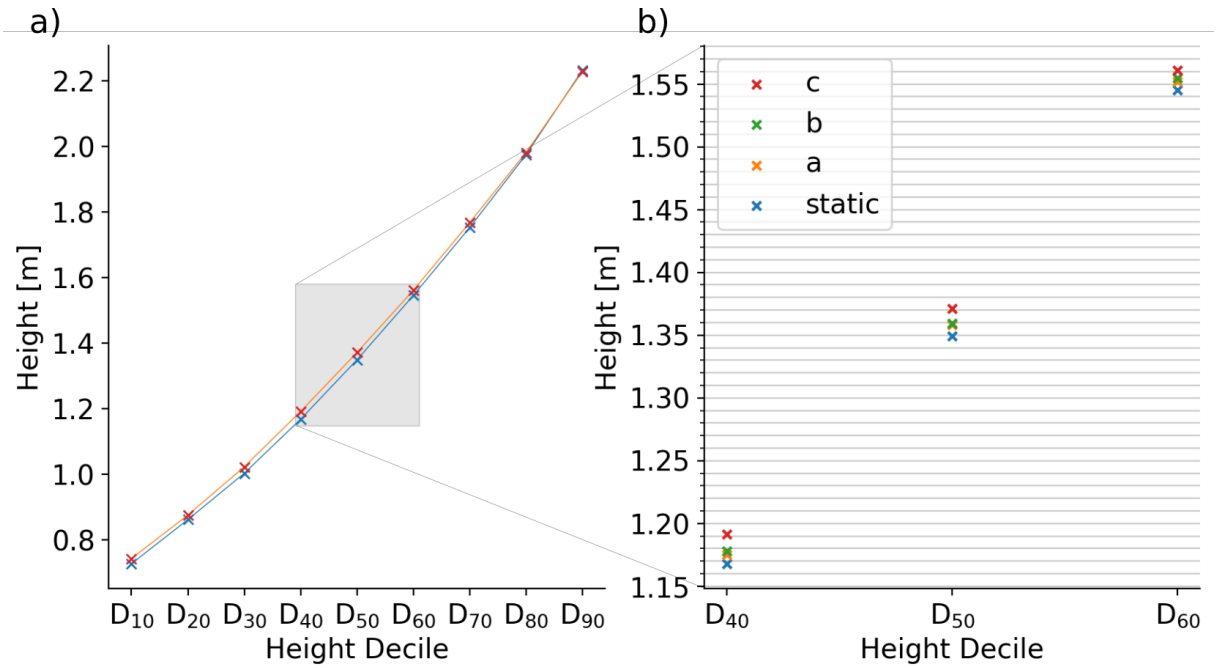

Figure 7: a) Height decile curves derived for simulated terrestrial laser scanning point clouds, averaged over the N=15 trees for the static scenario and motion scenario c. b) Zoomed in plot showing only the 4th, 5th and 6th height deciles for all four motion scenarios.

3.1.2 Voxel metrics

Figure 8 shows the voxel metrics, averaged over all trees (N=15), for three different voxel sizes for each scenario. The percentage of filled voxels is highest for the higher motion scenario c and lowest for the static scenario (Figure 8a). Conversely, the median number of points is highest for the static scenario and lowest for the motion scenario c (Figure 8b). While the differences between the static scenario and the light and moderate motion scenarios are small, the high magnitude motion scenario c clearly stands out. For the maximum number of points and the standard deviation of the number of points (Figure 8c and d), differences between the scenarios are small and depend on the voxel size. For the 5 cm voxel size, the values decrease slightly from the static scenario to the heavy motion scenario c. For the 10 cm voxel size the opposite is true and the values increase slightly. However, the effects are small.

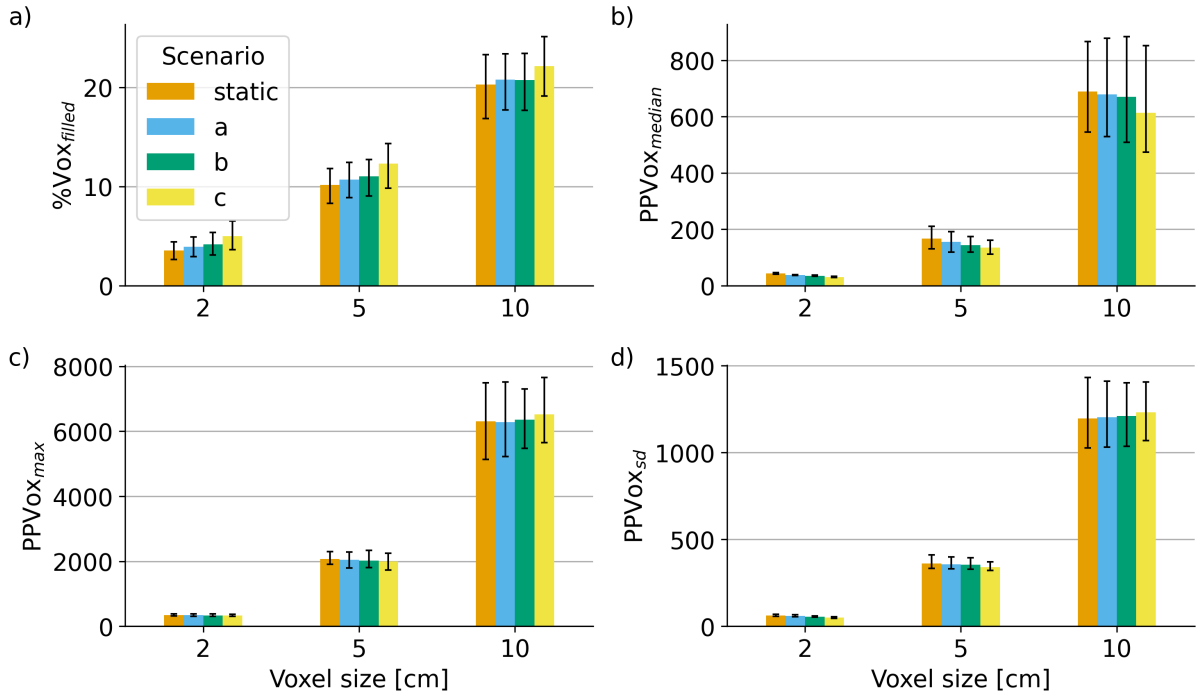

Figure 8: Voxel metrics estimated from simulated terrestrial laser scanning point clouds by voxel size and by motion scenario. a) Percentage of filled voxels (%Vox$_{filled}$), b) median number of points per voxel (PPVox$_{median}$), c) maximum number of points per voxel (PPVox$_{max}$) and d) standard deviation of points per voxel (PPVox$_{sd}$), averaged over all trees (N=15). The error bars show the interval between the 5th and the 95th percentile.

Filtering the point clouds with the SOR and MLS filters reduces the percentage of filled voxels in each scenario (Figure 9a and c) and increases the median number of points per voxel (Figure 9b and d). This confirms that the filtering reduces measurement noise in the point cloud. After filtering, the percentage of filled voxels is still highest for scenario c and the median number of points per voxel is still lowest for motion scenario c, so differences between the scenarios remain.

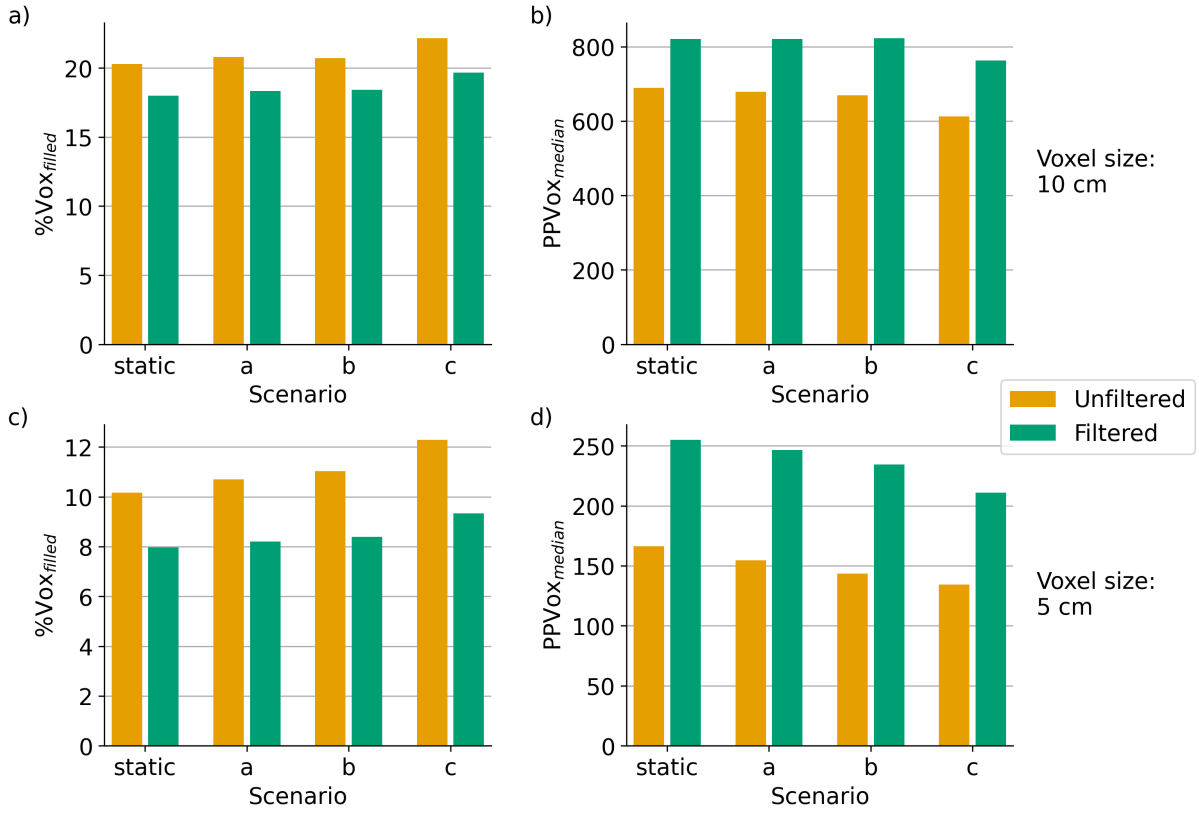

Figure 9: Comparison of voxel metrics estimated from simulated terrestrial laser scanning point clouds before (unfiltered) and after (filtered) the statistical outlier removal (SOR) and moving least squares (MLS) filters for voxel sizes of 10 cm (top row) and 5 cm (bottom row), averaged over all trees (N=15). a), c) Percentage of filled voxels ($\%Vox_{filled}$). b), d) Median number of points per voxel ($PPVox_{median}$). Note that the top and bottom y-axes are scaled differently.

3.1.3 Geometric features

The distributions of the four pointwise geometric features for the different motion scenarios are shown in Figure 10. We first look at the geometric features computed on the unfiltered point cloud (Figure 10, filled step histograms). Large effects of motion are observed for planarity P_{λ_3D} and sphericity S_{λ_3D}. As more leaf motion is introduced into the tree models, the distribution of P_{λ_3D} shifts to the left, i.e., to lower values, especially for the smaller search radius of 1 cm. For linearity L_{λ_3D}, the effect depends on the search radius. For the 1 cm radius, where the

distribution is right-skewed, there is little difference between the motion scenarios. For the 5 cm search radius, the distribution is closer to a normal distribution and it shifts to the left with more leaf movement. The sphericity distribution, again skewed to the right, shifts to the right as motion is introduced. This is true for both search radii. The distribution of verticality V_{λ_3D} is skewed to the right for the static scenario, but flattens out when motion is introduced. In the high motion scenario c, the distribution of V_{λ_3D} computed at a search radius of 5 cm is almost uniform.

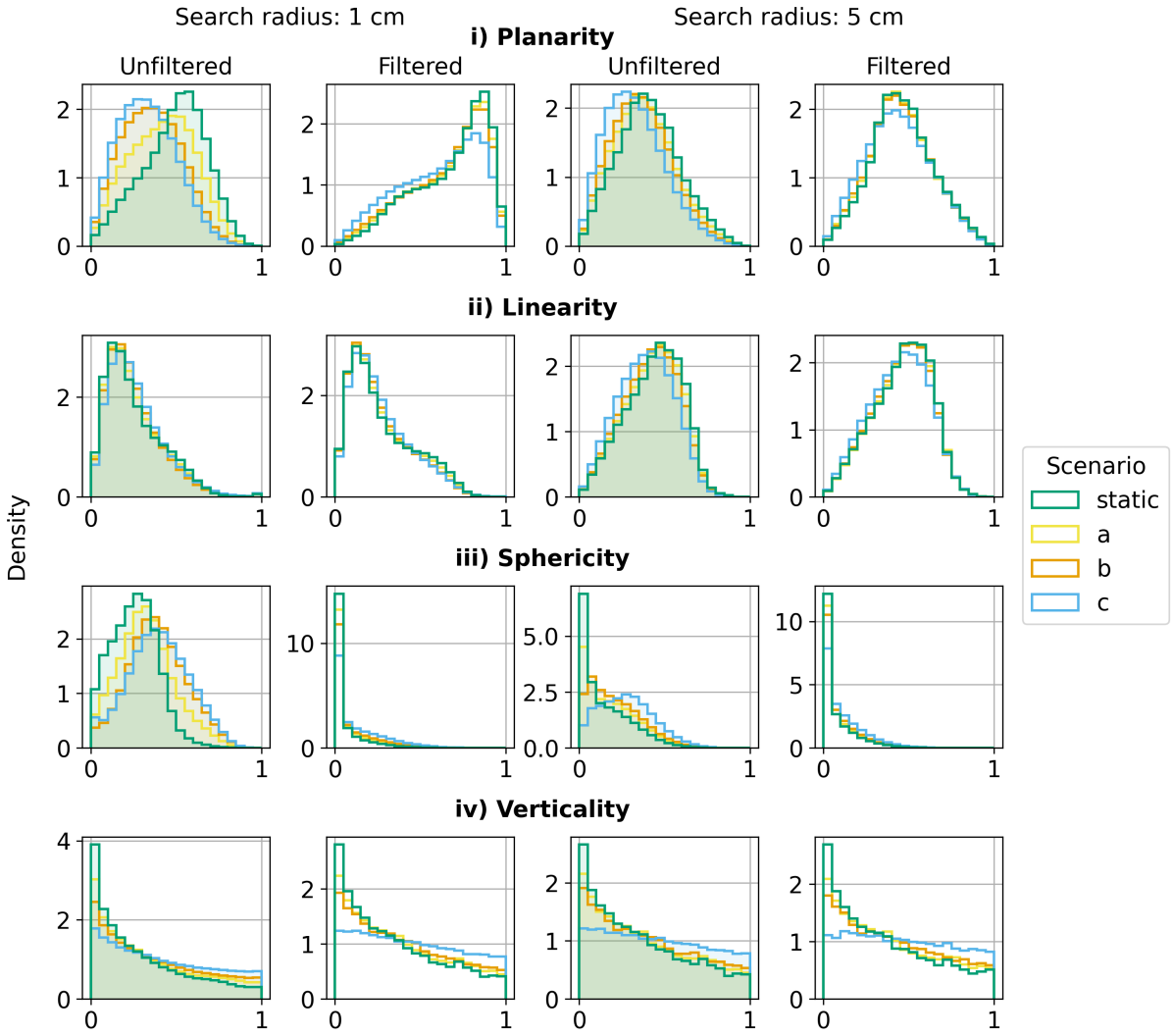

Figure 10: Density histograms of the geometric features i) planarity P_{λ_3D}, ii) linearity L_{λ_3D}, iii) sphericity S_{λ_3D}, and iv) verticality V_{λ_3D}, calculated for all leaf points of the simulated terrestrial laser scanning point (N=15) for two different spherical search radii before filtering (filled histograms) and after filtering (outlined histograms). The histograms are coloured by motion scenario.

After applying the MLS filter (Figure 10, outlined histograms), the differences between the motion scenarios are reduced for all geometric features. As a result of the MLS smoothing, leaf surface normals are harmonised, the distributions of planarity P_{λ_3D} shift to the right for both search radii, and the mean and median planarity values increase. The effect of filtering on

P_{λ_3D} is particularly strong for the 1 cm search radius, where the distribution becomes clearly skewed to the left. While the static scenario and scenarios a and b show very similar planarity distributions, the peak of the distribution is smaller in scenario c (Figure 10i, blue outlined histogram). The distributions of L_{λ_3D} are hardly affected by the point cloud filtering. For the 1 cm search radius, there are fewer values between 0.2 and 0.4 after filtering and more values between 0.5 and 0.8 (Figure 11ii). For the 5 cm search radius, filtering shifts the distributions slightly to the right and harmonises the distributions of the four motion scenarios. For S_{λ_3D} the distributions shift clearly to the left, with a majority of the values close to zero for all scenarios and for both search radii. As before filtering, the static scenario still has the highest density of low values and the heavy motion scenario the lowest density. For V_{λ_3D}, noticeable differences between the scenarios remain after SOR and MLS filtering. Especially for the 5 cm search radius, the SOR and MLS filters do not significantly change the distribution of V_{λ_3D}. For the 1 cm search radius, the modes of the distribution become smaller compared to the pre-filter version.

Furthermore, the unfiltered point clouds have on average between 14 150 (static scenario) and 15 450 (scenario c) NoData values at the 1 cm search radius, which is around 0.27% of all points. These values indicate that there were not enough points present in the search sphere for the principal component analysis used to estimate the geometric features. For the 5 cm search radius, there are between 200 (scenario c) and 252 (static scenario) NoData values on average. However, after MLS filtering, there are only between 205 (static scenario) and 658 (scenario c) NoData values when calculated with a 1 cm search radius and between 2 and 7 NoData values when calculated with a 5 cm search radius.

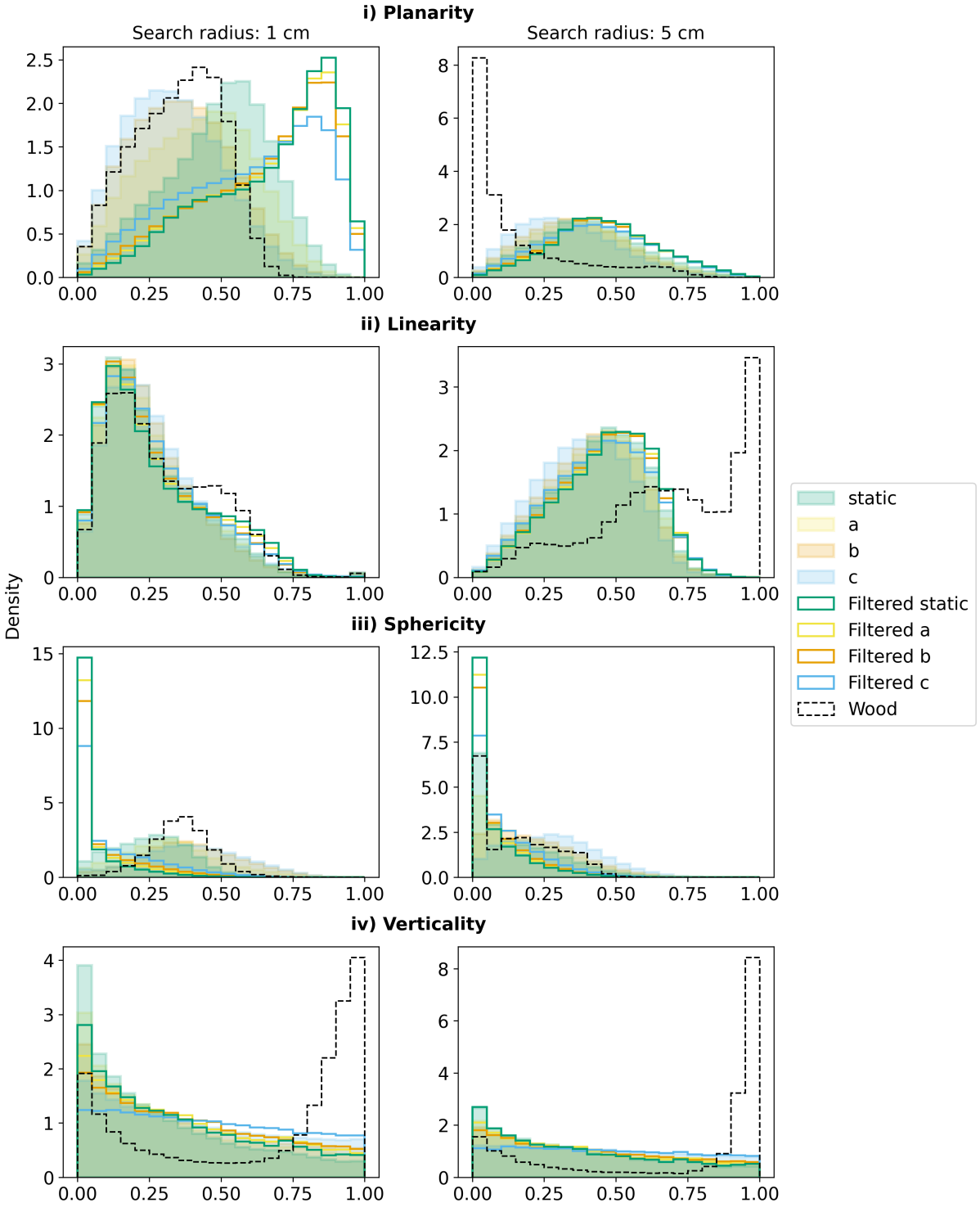

Figure 11: Density histograms of the geometric features i) planarity P_{λ_3D}, ii) linearity L_{λ_3D}, iii) sphericity S_{λ_3D}, and iv) verticality V_{λ_3D}, calculated from the terrestrial laser scanning point clouds (N=15) for two different spherical search radii. The filled histograms show the distribution of features for leaf points before filtering, the outlined histograms show the distribution of features after filtering. The colours indicate the motion scenario. The black dashed histograms show the distribution of features calculated from the wood point cloud (static scenario).

3.1.4 Leaf area

Reference leaf area (LA) was retrieved for each input tree model by summing up the areas of the faces that make up the leaves. These values are used to assess the accuracy of the estimated leaf area derived using the alpha shape method, the 2.5D Delaunay triangulation method, and the 3D Poisson surface reconstruction method (both with and without the MLS filter) and the light transmission/attenuation based estimators (only without the MLS filter) on a per tree basis. The relative differences to the reference, i.e., the percentage errors, are displayed as violin plots in Figure 12. Reference LA values are between 0.44 m^2 and 1.53 m^2.

All geometric methods overestimate LA from the unfiltered point clouds even in the static scenario, and leaf motion leads to increased overestimation (Figure 12a). 2.5D Delaunay triangulation results in the greatest overestimation for the unfiltered data. It is also the most sensitive to leaf motion, with a mean overestimation of 116 % in the static scenario, and 226 %, 321 %, and 497 % in the motion scenarios a, b, and c, respectively (about 1.2 m^2 to 4.9 m^2 in absolute numbers). Poisson surface reconstruction is the most accurate method for the unfiltered data (mean overestimation between 18 % in the static scenario and 111 % in scenario c). The alpha shape method gives almost comparable results, but the overestimation is slightly higher (mean percentage error of 52 % in the static scenario and 118 % in scenario c). LA_{α} is slightly less sensitive to leaf motion with 0.63 m^2 between the mean absolute errors in the static scenario and scenario c compared to 0.89 m^2 for $LA_{poisson}$.

The indirect LA estimates with AMAPVox are more accurate, with mean percentage errors below 40 % for all estimators. The differences between the estimators are greater than the differences between the motion scenarios, with the transmittance-based estimations closest to the reference with our chosen settings (Figure 12b). For the attenuation-based estimators, there is a small increase in the mean error with increasing motion. The most notable difference is between scenario c and the other scenarios. The differences in the means are 0.035 m^2 (LA_t), 0.066 m^2 (LA_{att_ppl}), and 0.122 m^2 (LA_{att_fpl}) between the static scenario and scenario c. These small differences are statistically significant at the 95% confidence level (paired t-tests between static scenario and scenario c: i) LA_t: $t(14) = -3.902$, $p = .0016$, ii) LA_{att_ppl}: $t(14) = -5.937$, $p < .001$, iii) LA_{att_fpl}: $t(14) = -9.357$, $p < .001$).

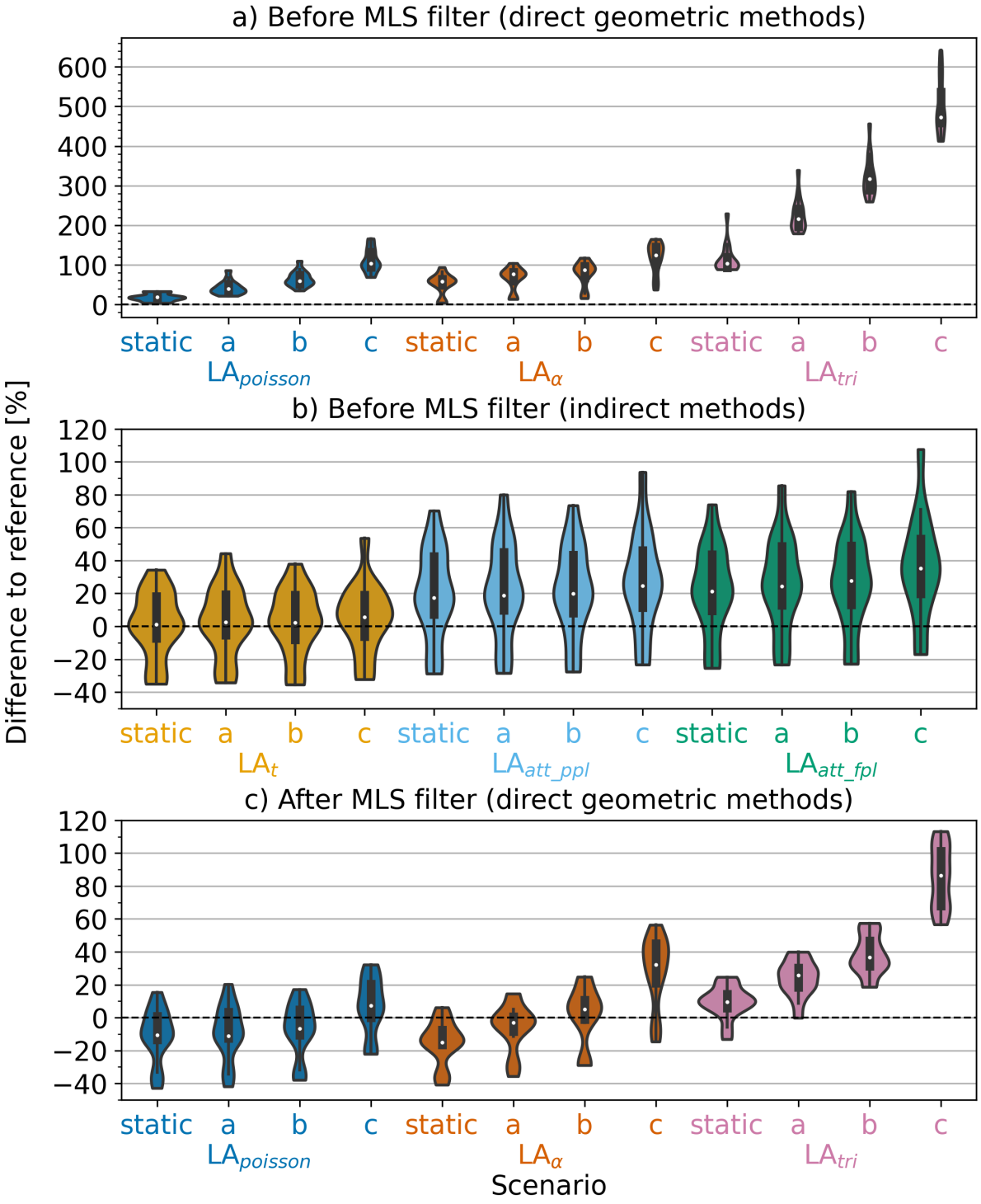

Figure 12: Violin plots showing the relative difference between estimated leaf area (LA) and true LA derived from the simulated terrestrial laser scanning point clouds of the N=15 trees in the four motion scenarios a) before moving least squares (MLS) filtering with the different geometric methods, b) before MLS filtering with the indirect light transmission based methods, and c) after MLS filtering with the geometric methods (see Table 6 for an overview of the metrics).

The filtering procedure with the SOR and MLS filters improves the estimates of all three geometric methods (Figure 12c). Mean relative errors go down to about −11 % to 11 % for $LA_{poisson}$, −15 % to 32 % for LA_{α} and 10 % to 86 % for LA_{tri}. The Poisson surface reconstruction method slightly underestimates the actual LA after MLS filtering (except in scenario c), while the mean errors of the LA estimates calculated with the 2.5D Delaunay triangulation method remain positive for each scenario. With the alpha shape method, LA is underestimated in scenarios static and a, and overestimated in scenarios b and c. Overall, the differences between the methods decrease significantly, as do the differences between the scenarios. Still, for the alpha shape and the 2.5D Delaunay triangulation, mean LA increases with leaf motion (by 0.41 m^2 and 0.75 m^2 between static and c, respectively), whereas for the Poisson surface reconstruction there is only a difference of 0.18 m^2 between the means of the static scenario and scenario c.

For both the indirect light transmission based methods (Figure 12b) and the direct geometric methods after MLS resampling (Figure 12c), the tails of the density curves indicate that there are a couple of trees for which LA is underestimated considerably. Looking at the data, we see that these are trees 6 and 7, which have in common that their leaves all grow at the last branching level and share the same leaf base (Figure 2).

3.2 Effect of point cloud filtering on real data

To further investigate the effects of MLS filtering, we also calculate point cloud metrics on a real TLS point cloud of an apple tree (Section 2.1.2). Note that in this experiment the pre-filter point cloud has already been cleaned with the SOR filter (Section 2.1.2).

The height metrics do not differ notably between the unfiltered and filtered point clouds. The voxel-based metrics behave similarly to the simulated data, with a decrease in $\%Vox_{filled}$ and an increase in $PPVox_{median}$, but the differences are less pronounced (Figure 13).

Geometric features are shown in Figure 14 for the leaf points before (filled histograms) and after filtering (outlined histograms) and for the wood points (dashed histograms). The distributions of the geometric features of leaf points in the real point cloud before filtering mostly resemble the distributions in motion scenario c in the simulated dataset. The distribution of planarity values has an even stronger right skew than any of the simulated scenarios. MLS smoothing changes the distributions of all four geometric features in a similar way than in the simulated point clouds (cf. Figure 11).

No reference LA measurements are available for the real tree. Therefore, we can only compare the different estimation methods and observe the influence of MLS filtering, but cannot make an absolute statement about the accuracy of the derived values. On the unfiltered point cloud, the lowest LA estimates are obtained with the alpha shape algorithm (1.721 m^2). LA obtained with 2.5D Delaunay triangulation is more than six times higher with 10.575 m^2 (Table 8). As for

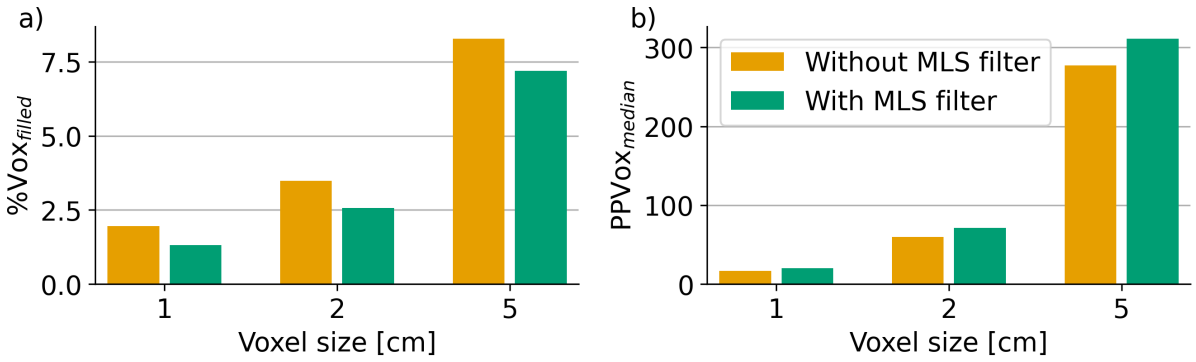

Figure 13: Voxel metrics estimated from the real terrestrial laser scanning point cloud by voxel size before and after moving least squares (MLS) filtering. a) Percentage of filled voxels (%Vox$_{filled}$), b) median number of points per voxel (PPVox$_{median}$).

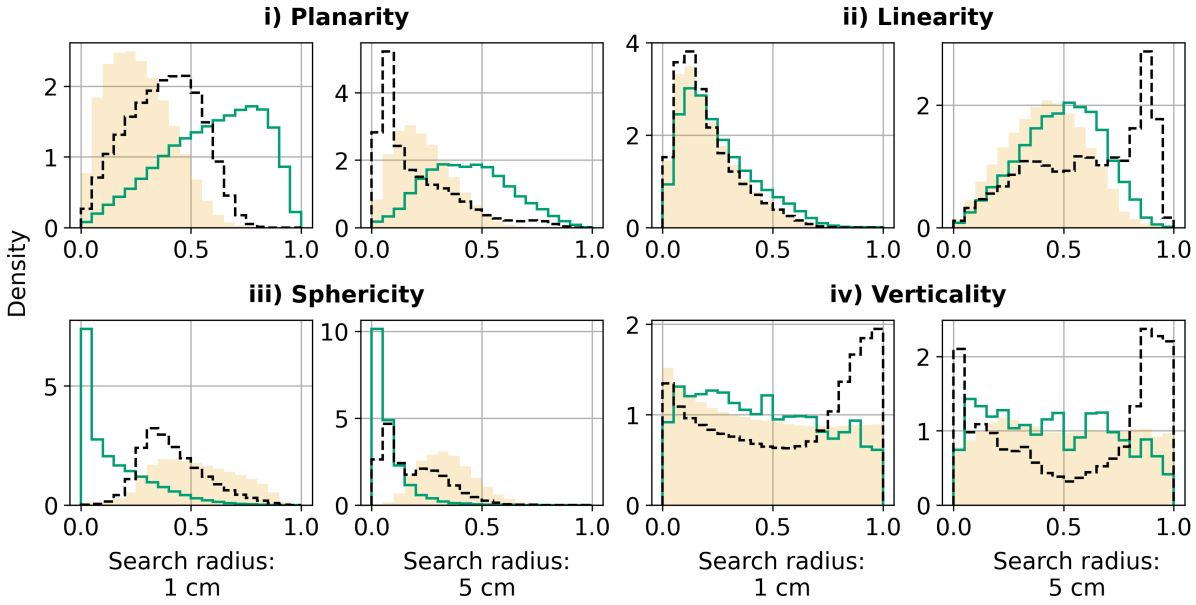

Figure 14: Density histograms of the geometric features i) planarity P_{λ_3D}, ii) linearity L_{λ_3D}, iii) sphericity S_{λ_3D}, and iv) verticality V_{λ_3D}, calculated from the real terrestrial laser scanning tree point cloud for two different spherical search radii. The filled histograms show the distribution of features before filtering the point clouds, the unfilled step histograms show the distribution of features after filtering the point clouds, and the black dashed histograms show the distribution of features calculated from the wood points.

the synthetic trees, all LA estimates are lower after applying the MLS filter. $LA_{poisson}$ and LA_{α} agree very well with a difference of only 0.057 m^2. After filtering, LA_{tri} is still around 0.8 m^2 than the other two LA estimates. MLS filtering leads to the largest reduction in estimated leaf area for the 2.5D Delaunay triangulation method (LA_{tri}) with 8.73 m^2 compared to 1.43 m^2 for the Poisson surface reconstruction method and only 0.67 m^2 for the alpha shape method (Table 8).

Table 8: Leaf area (LA) estimates from the real terrestrial laser scanning point cloud with the three direct geometric methods (Poisson surface reconstruction $LA_{poisson}$, alpha shapes LA_{α}, 2.5D Delaunay triangulation LA_{tri}) before and after filtering with moving least squares (MLS).

Leaf area	Estimate before MLS filter	Estimate after MLS filter	Difference
$LA_{poisson}$	2.413 m^2	0.955 m^2	1.458 m^2
LA_{α}	1.721 m^2	1.044 m^2	0.677 m^2
LA_{tri}	10.575 m^2	1.842 m^2	8.733 m^2

3.3 Metrics derived from UAV-borne laser scanning (ULS) point clouds

The simulated ULS tree point clouds in the static scenario have an average of 2432 points, 359 wood points and 2073 leaf points. The difference in the average number of wood and leaf points between the motion scenarios is no more than 3. There is also barely any difference between the point clouds in terms of height metrics such as mean height and height deciles. Figure 15 shows the ULS point clouds of tree 1 simulated in the different scenarios side by side.

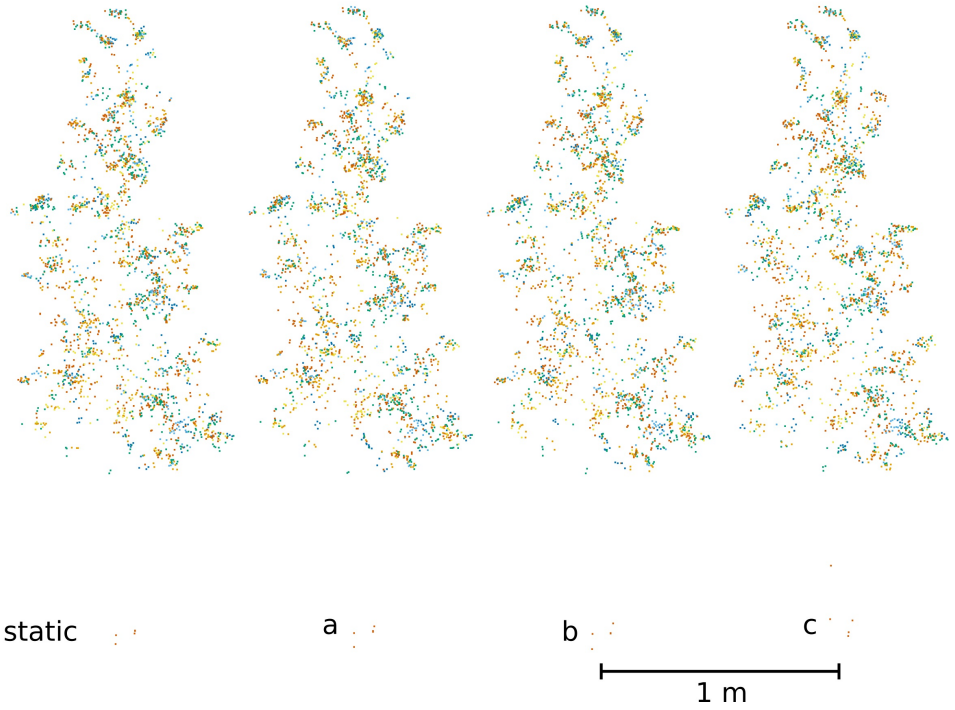

Figure 15: Comparison of UAV-borne laser scanning tree point clouds for tree 1 simulated in the four different motion scenarios, coloured by point source ID (i.e., flight line).

Figure 16 shows the voxel metrics, calculated for three different voxel sizes. Again, there are only small differences that do not seem to be related to the leaf motion scenario.

For leaf area (Figure 17), there are some differences between the estimation methods. The transmittance estimator and the free path length (FPL) estimator of the attenuation coefficient (with bias correction) are very accurate in terms of the mean and median error, while the potential path length (PPL) estimator slightly underestimates leaf area (mean absolute error = $-0.1\,\mathrm{m}^2$). The differences between the motion scenarios are minimal and show no statistical significance at the 0.05 significance level (paired t-tests between static scenario and scenario c: i) LA_t: $t(14)$ = -0.146, p = .886, ii) LA_{att_ppl}: $t(14)$ = 0.145, p = .887, iii) LA_{att_fpl}: $t(14)$ = -0.233, p = .819).

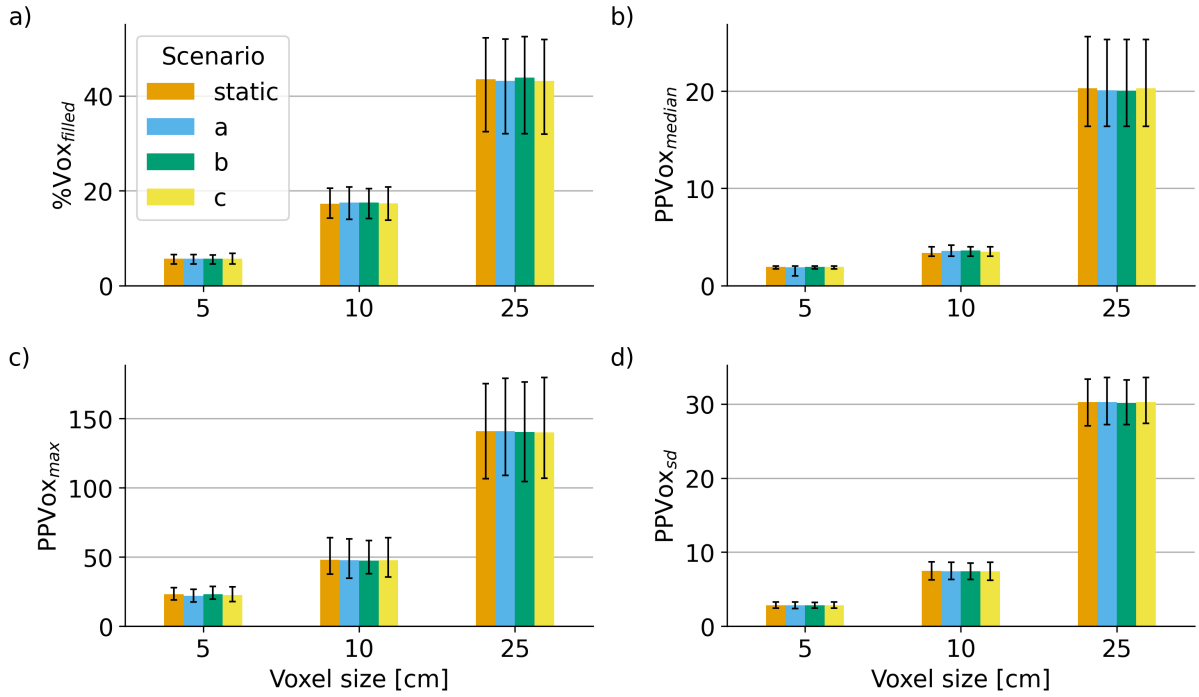

Figure 16: Voxel metrics estimated from simulated UAV-borne laser scanning point clouds by voxel size and by motion scenario. a) Percentage of filled voxels (%Vox$_{filled}$), b) median number of points per voxel (PPVox$_{median}$), c) maximum number of points per voxel (PPVox$_{max}$) and d) standard deviation of points per voxel (PPVox$_{sd}$), averaged over all trees (N=15). The error bars show the interval between the 5th and the 95th percentile.

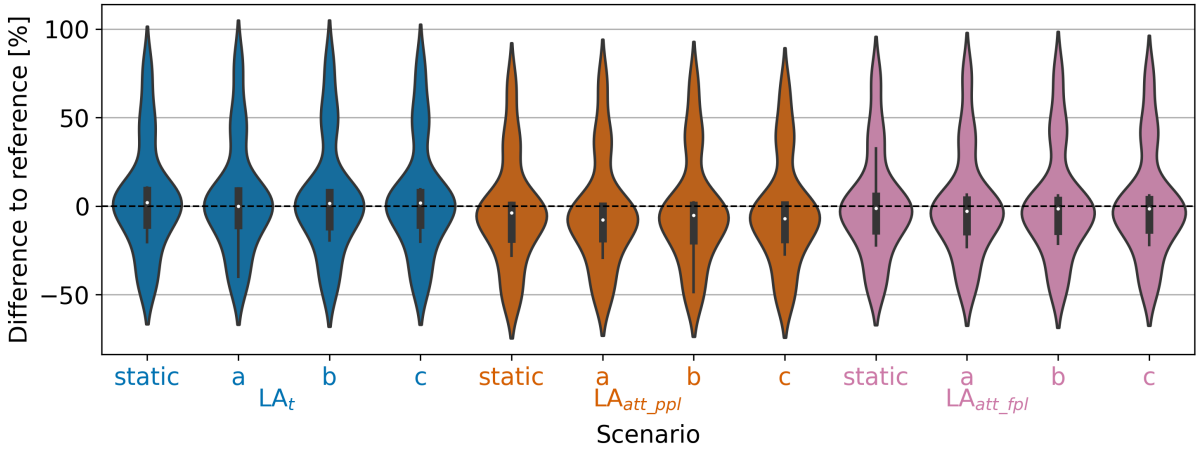

Figure 17: Violin plots showing the relative difference between estimated leaf area (LA) and true LA derived from the simulated UAV-borne laser scanning point clouds with different estimators implemented in AMAPVox (see Table 6) for the N=15 trees in the four motion scenarios.

4 Discussion

The discussion is organised as follows: Firstly, we analyse the effects of vegetation movement when comparing TLS and ULS platforms. Subsequently, we investigate the sensitivity of the different metrics to leaf motion and discuss the potential of employing filtering procedures on TLS point clouds to mitigate motion effects. Moreover, we propose further improvements in virtual laser scanning of dynamic scenes. Finally, we broaden the scope and discuss the opportunities of leveraging VLS of dynamic vegetation scenes for method development and machine learning.

4.1 Effect of leaf motion depending on acquisition platform

In line with our hypothesis, our research has shown that the motion of individual leaves clearly affects the metrics computed from TLS point clouds, but has no significant effect on the metrics derived from ULS point clouds. This can be explained by the differences in resolution and viewing geometry (Morsdorf et al., 2017). In the simulated TLS point clouds, a single leaf is sampled by several hundred, often more than 1000 points. In the ULS point clouds, there are typically less than 10 points per leaf. Furthermore, the sensors have different ranging accuracies and laser beam footprints. With a measurement range accuracy of 0.01 m (RIEGL LMS, 2023) and leaf movement in the range of only a few centimetres, it is almost impossible to distinguish between measurement error and leaf movement.

4.2 Sensitivity of metrics to leaf motion

Comparing the simulated TLS point clouds with different levels of motion, we find notable differences in the total number of points and the number of leaf and wood points. The increase in leaf points with greater motion is quantitative evidence for the presence of 'twin' leaves in the point cloud. In the point clouds of trees with moving leaves, more space is filled with leaf points than in the static point cloud, because the leaves are captured in different states with different orientations. This is also reflected in the higher proportion of filled voxels (Figure 8). At the same time, the number of wood points decreases with leaf motion, indicating that wood parts are increasingly occluded by leaves. These effects are rather moderate for our scenes, which contain only a single tree with a maximum height of 3 m and a rather sparse crown. We expect this effect to be more significant for taller trees and in forest settings with dense canopies. This can be a problem when the woody structure is of interest, e.g., for TLS-based volume and biomass estimation based on quantitative structure models (QSMs). Here, low

point density and occlusions in the upper crown are already known problems (Calders et al., 2020).

In terms of geometric features computed on leaf points, notable differences can be observed between different levels of motion, especially for planarity at the 1 cm search radius and for sphericity. This may be relevant for supervised machine learning-based leaf-wood separation based on geometric features (Wang et al., 2017; Xi et al., 2020). The comparison of geometric features between leaf and wood points (Figure 11) highlights the importance of choosing a search radius where the geometric features of leaf and wood points differ, or ideally using multiple search radii (J. Zhou et al., 2019). The results also suggest that accuracy and transferability of machine learning-based leaf-wood separation models can be enhanced by also including training samples of moving leaves (with different magnitudes). The differences in geometric features between point cloud representations of static and of moving leaves may also be useful for classifying non-moving and moving tree parts.

Leaf area estimation in TLS point clouds based on direct geometric methods is very sensitive to leaf motion (Section 3.1.4). For each of the three methods we tested (2.5D Delaunay triangulation, alpha shapes and Poisson surface reconstruction), leaf area is increasingly overestimated as leaf motion increases. For true leaf areas between 0.44 m^2 and 1.53 m^2, the observed overestimation of around half a metre (Poisson surface reconstruction and alpha shapes) or even several metres (2.5D Delaunay triangulation) is not acceptable for most applications. In contrast, the indirect methods based on local light extinction, quantified per voxel, are very robust to leaf flutter during point cloud acquisition (difference in relative errors below 15 %; Figure 12b). Of the geometric methods, Poisson surface reconstruction is the least sensitive to leaf motion, followed by the alpha-shape method. 2.5D Delaunay triangulation based on the best fitting plane drastically overestimates the leaf area by almost 100% in the static scenario and by more than 400% in motion scenario c (Figure 12a). Both Poisson surface reconstruction and alpha shapes have the advantage over the 2.5D Delaunay triangulation that no prior leaf segmentation is required. This reduces the number of processing steps required. 2.5D Delaunay triangulation, in contrast, is highly dependent on the quality of the leaf segmentation. In particular undersegmentation of leaves (i.e., several leaves in one segment) can result in drastic overestimation of leaf area. In the case of our simulated point clouds, where we use the HELIOS++ point cloud attribute 'object ID' to distinguish individual leaves, multiple leaf representations are treated as a single leaf surface in the moving scenario and the triangulated surface is therefore overestimated.

As noted by Moon et al. (2022), these geometric leaf area estimation methods are usually very sensitive to their parameters. Leaf point clouds acquired in almost windless conditions may require different parameter settings to those acquired in windy conditions. VLS can assist in finding the optimal parameters for the point cloud under investigation, given that the tree structures and wind conditions can be reflected reasonably well in the virtual 3D scenes. VLS can also help help to find the correct settings for indirect LA estimation with AMAPVox, which is particularly sensitive to voxel size, by simulating laser scanning over virtual trees or forests that resemble the real-world study area.

Although not investigated quantitatively in this work, we assume that the observed effects in the metrics derived from the simulated multi-scan TLS point clouds are due to leaf movement between scans, but not within scans. Visual comparisons did not reveal any discernible differences in leaf representation between the single scans (as opposed to the merged point clouds) of the static and moving scenarios.

4.3 The potential of filtering procedures

The statistical outlier removal (SOR) filter helps to remove isolated points caused by partial hits, resulting in a cleaner point cloud. However, it cannot remove multiple 'twin' leaves occurring due to leaf flutter during scan acquisition. In this context, Boukhana et al. (2022) found that the SOR filter alone does not improve the accuracy and robustness of geometric LA estimation methods. Unlike the SOR filter, the MLS filter does not remove points and leave the other points untouched, but rather smoothes and resamples the point clouds, thus changing the positions of the points (Figure 4). By harmonising the normals of the local surface, the MLS filter leads to a change in geometric features (Figure 10, Figure 11), in particular planarity (at the 1 cm search radius) and sphericity. This can be useful for certain analyses, such as estimating leaf angle distribution or performing leaf separation. As shown in Figure 10, the differences between the motion scenarios in terms of geometric features decrease considerably. Furthermore, the leaf area estimates become more accurate through filtering and the differences between the scenarios are reduced. This shows that the MLS filter can successfully mitigate motion effects to a certain degree, as suggested by Yun et al. (2016). This is consistent with Boukhana et al. (2022), who report improved accuracy and robustness of their tested geometric leaf area estimation methods with the MLS filter.

After filtering, the direct geometric LA estimation methods almost consistently underestimate the leaf areas of trees 6 and 7 (Figure 12b and c). These trees have in common that their leaves grow at the last level of branching, which leads to leaf clumping. As a result, the MLS filter not only smooths out the different twin occurrences of a single leaf, but also merges separate leaves into one surface. This leads to underestimation of LA. We assume that leaf clumping can also explain the underestimation of leaf area for trees 6 and 7 with the indirect light extinction based methods with AMAPVox (Vincent et al., 2017) (Figure 12b). These findings show that the effects of movement and also of point cloud filtering depend on tree and leaf morphology, which requires further investigation, e.g., by VLS of a larger diversity of dynamic trees.

Overall, filtering the leaf points with MLS reduces measurement noise and movement effects and is an effective approach for improving leaf area estimates with direct geometric methods.

4.4 Further development of virtual laser scanning (VLS) of dynamic scenes

The presented research on the influence of tree movement during point cloud acquisition on the derived information could be extended to larger scenes and other acquisition platforms. Typically, trees are embedded in a surrounding, such as an orchard or a forest. By modelling whole orchards or forest plots, laser scanning simulations of dynamic scenes could consider further effects such as occlusion by adjacent and overlapping tree crowns. It would be interesting to explore further acquisition platforms, such as mobile laser scanning from tractors or conveyor belts, as in precision agriculture, or SLAM (simultaneous location and mapping) based handheld or backpack laser scanning, as in forestry.

While the HELIOS++ simulations of dynamic scenes with leaf flutter could be processed in reasonable time, simulations with high spatial and temporal resolution will require enormous computation times when larger scenes (e.g., entire forest plots) with more moving objects are introduced. Improvements in the KDTree data structure for handling the moving scenes and the ray intersections will allow for larger and more sophisticated scenes and motions (Esmoris et al., 2022).

To simplify the geometry, i.e., to keep the number of triangles low, leaves have been modelled as flat hexagons in this work. In reality, leaves have more complex shapes and can be lobed, have dentate or serrate margins, or be arranged in compounds. Leaves also have some degree of curvature. More realistic 3D tree models could include curved leaves of more complex shapes. These could be created by hand, using automated rule-based approaches, or by deep learning. For instance, Boukhana et al. (2022) developed a method to generate synthetic leaf point clouds based on nine criteria, relating to the shape of the leaf and to defects in the point cloud due to the acquisition process. Moon et al. (2022) used deep generative models to generate point clouds of sweet pepper leaves.

The current HELIOS++ parameters for defining the speed of the virtual rigid motions (`dynStep` and `kdtDynStep`) are relative to the simulation frequency, i.e., the pulse frequency used by the scanner. This means that when using different acquisition settings, these dynamic step parameters may need to be adjusted to take account of the simulation frequency. In order to make the configuration of the speed of the virtual motions easier and more flexible, dynamic time step parameters should be introduced in addition to the current parameters. These dynamic time step parameters would allow specifying the time step per simulation step (in virtual time) directly, which allows the same scene to be used for surveys with completely different simulation frequencies.

In this study, animations of leaf flutter were created in the 3D computer graphics software Blender by applying rotations to the leaves. In terms of tree movement, the study could be extended to include not only leaf flutter, but also branch buffeting, i.e., the elastic response of branches to wind turbulence (Tadrist et al., 2018). This would add considerable complexity to

the virtual scene by combining branch motion and leaf flutter. At present, this would be difficult to parameterise in a HELIOS++ XML file using only combinations of rigid motions. For many applications, however, it will be sufficient to work with snapshots of a dynamic scene, which will be exchanged between single acquisitions (e.g., scan positions). Several physics-based wind simulation methods have been presented in the literature that can be used to generate a time series of mesh models for a given wind field (Pirk et al., 2014; Xu et al., 2020). Higher magnitudes of wind-induced tree movement would then also be visible in lower resolution point clouds, i.e. ULS point clouds. These wind simulations may also be applied to QSM models generated from real TLS point clouds instead of synthetic tree models, as already demonstrated by Jackson et al. (2019). As an alternative to physically based wind simulations, tree movement could also be derived from real trees, e.g., from high-resolution TLS time series or from videos or multiple images. For example, Kattenborn et al. (2022) predicted the temporal variation of leaf angle distributions from image series, which could be used to parameterise dynamic scenes in VLS.

4.5 The potential of dynamic vegetation scenes

Due to the need for large training datasets, machine learning and especially deep learning applications are increasingly using synthetic and simulated data to train the models, e.g., for semantic segmentation to separate leaf and wood in laser scanning point clouds (Morel et al., 2020). Here, using simulated data which includes the effects of vegetation movement (and potentially other error sources such as alignment errors), may increase the accuracy and transferability of the trained model. We therefore believe that VLS of dynamic scenes can be a means of bridging the reality gap between real and simulated laser scanning data, and can improve VLS-based or VLS-assisted machine learning models.

As a simple indicator of the realism of simulated point clouds, the distribution of geometric features can be used. In our experiment (Section 3.2), the distribution of geometric features in the simulated data matches the distribution in the real point cloud quite well. The comparison of real data and simulated data confirms that our real tree, which was acquired under moderately windy conditions, is closer to the simulated point clouds in the motion scenario c than in the static scenario. To turn it around, this suggests that our moving scenarios produce more realistic VLS point clouds than the static scenario. However, the distributions of the geometric features in real versus simulated point clouds can also be explained by the more complex leaf shape and the leaf curvature in the real data (Section 4.4), resulting in lower local planarity and higher sphericity values.

With the advancement of 4D applications (3D + time) such as high frequency or permanent laser scanning for vegetation monitoring (Campos et al., 2020), algorithms need to be developed to extract information from these multitemporal datasets (Puttonen et al., 2016; Puttonen et al., 2019; py4dgeo Development Core Team, 2022) that go beyond pairwise bitemporal change detection (cf. Anders et al., 2021 for topographic surface changes). Realistic 4D virtual laser

scanning data of vegetation can be useful for testing these novel algorithms, while having perfect reference data available. Once the different processes are better understood and can be modelled in space and time, deep learning models trained on VLS data with dynamic vegetation scenes may enable future methods to disentangle different processes and rhythms of vegetation movement, such as diurnal patterns, seasonal patterns, growth, or drought stress-related changes.

5 Conclusion

This research presents a proof of concept of how virtual laser scanning (VLS) can be used to investigate the influence of vegetation movement on commonly used point cloud metrics. We found that wind-induced leaf flutter is relevant in high-resolution laser scanning data with delayed measurements from different positions, such as terrestrial laser scanning (TLS), but is negligible in typical UAV-borne laser scanning (ULS) applications. In the case of TLS data, we found that standard height metrics and height deciles, as well as indirect leaf area (LA) estimates based on light extinction, are robust to leaf flutter. Higher levels of leaf flutter lead to more leaf points and fewer wood points, as well as a higher percentage of filled voxels, indicating increased occlusion by leaves when leaves are moving. The distributions of geometric features of leaf points (especially planarity and sphericity) and direct geometric LA estimation methods are also sensitive to leaf motion. LA errors are up to five times higher in the scenario with heavy leaf motion than in the static scenario. Filtering the leaf points in TLS point clouds with moving least squares (MLS) surface approximation significantly improves the accuracy of LA estimation with geometric methods. Even for the most accurate method, Poisson surface reconstruction, mean relative errors decrease from between 20 % (static scenario) and 110 % (heavy motion scenario) to between −10 % to 10 %. Filtering also reduces the differences in the distributions of geometric features between the leaf motion scenarios. Building on our work, dynamic VLS of vegetation should be further developed by including more sophisticated and realistic leaf shapes and tree movements, larger scenes with overlapping and interacting trees, and additional acquisition platforms. This will make VLS of dynamic vegetation scenes a powerful method for the development of algorithms to analyse 4D vegetation time series.

Bibliography

Åkerblom, M., & Kaitaniemi, P. (2021). Terrestrial laser scanning: a new standard of forest measuring and modelling? *Annals of botany*, *128*(6), 653–662. https://doi.org/10.1093/aob/mcab111

Alexa, M., Behr, J., Cohen-Or, D., Fleishman, S., Levin, D., & Silva, C. (2003). Computing and rendering point set surfaces. *IEEE Transactions on Visualization and Computer Graphics*, *9*(1), 3–15. https://doi.org/10.1109/TVCG.2003.1175093

Anders, K., Winiwarter, L., Mara, H., Lindenbergh, R., Vos, S. E., & Höfle, B. (2021). Fully automatic spatiotemporal segmentation of 3D LiDAR time series for the extraction of natural surface changes. *ISPRS Journal of Photogrammetry and Remote Sensing*, *173*, 297–308. https://doi.org/10.1016/j.isprsjprs.2021.01.015

Béland, M., Baldocchi, D. D., Widlowski, J.-L., Fournier, R. A., & Verstraete, M. M. (2014). On seeing the wood from the leaves and the role of voxel size in determining leaf area distribution of forests with terrestrial LiDAR. *Agricultural and Forest Meteorology*, *184*, 82–97. https://doi.org/10.1016/j.agrformet.2013.09.005

Blender Online Community. (2022). Blender - a 3D modelling and rendering package (version 3.4.0). Retrieved 2022-01-13, from https://www.blender.org/

Boukhana, M., Ravaglia, J., Hétroy-Wheeler, F., & de Solan, B. (2022). Geometric models for plant leaf area estimation from 3D point clouds: A comparative study. *Graphics and Visual Computing*, *7*, 200057. https://doi.org/10.1016/j.gvc.2022.200057

Bschorr, O. (1991). Winderregte Blattschwingungen. *Naturwissenschaften*, (78), 402–407. https://link.springer.com/content/pdf/10.1007/BF01133411.pdf

Calders, K., Adams, J., Armston, J., Bartholomeus, H., Bauwens, S., Bentley, L. P., Chave, J., Danson, F. M., Demol, M., Disney, M., Gaulton, R., Krishna Moorthy, S. M., Levick, S. R., Saarinen, N., Schaaf, C., Stovall, A., Terryn, L., Wilkes, P., & Verbeeck, H. (2020). Terrestrial laser scanning in forest ecology: Expanding the horizon. *Remote Sensing of Environment*, *251*, 112102. https://doi.org/10.1016/j.rse.2020.112102

Calders, K., Brede, B., Newnham, G., Culvenor, D., Armston, J., Bartholomeus, H., Griebel, A., Hayward, J., Junttila, S., Lau, A., Levick, S., Morrone, R., Origo, N., Pfeifer, M., Verbesselt, J., & Herold, M. (2023). StrucNet: a global network for automated vegetation structure monitoring. *Remote Sensing in Ecology and Conservation*. https://doi.org/10.1002/rse2.333

Campos, M. B., Litkey, P., Wang, Y., Chen, Y., Hyyti, H., Hyyppä, J., & Puttonen, E. (2020). A Long-Term Terrestrial Laser Scanning Measurement Station to Continuously Monitor Structural and Phenological Dynamics of Boreal Forest Canopy. *Frontiers in plant science*, *11*, 606752. https://doi.org/10.3389/fpls.2020.606752

CloudCompare. (2022). CloudCompare (version 2.12.0, Kyiv). Retrieved 2022-09-01, from https://www.cloudcompare.org/

Computree group. (2020). Computree. Retrieved 2023-01-06, from https://computree.onf.fr/?page_id=42

Côté, J.-F., Widlowski, J.-L., Fournier, R. A., & Verstraete, M. M. (2009). The structural and radiative consistency of three-dimensional tree reconstructions from terrestrial lidar. *Remote Sensing of Environment*, *113*(5), 1067–1081. https://doi.org/10.1016/j.rse.2009.01.017

D. J. Watson. (1947). Comparative Physiological Studies on the Growth of Field Crops: I. Variation in Net Assimilation Rate and Leaf Area between Species and Varieties, and within and between Years. *Annals of botany*, *11*(41), 41–76. Retrieved 2023-03-12, from http://www.jstor.org/stable/42907002

Demol, M., Wilkes, P., Raumonen, P., Krishna Moorthy, S., Calders, K., Gielen, B., & Verbeeck, H. (2022). Volumetric overestimation of small branches in 3D reconstructions of Fraxinus excelsior. *Silva Fennica*, *56*(1). https://doi.org/10.14214/sf.10550

Disney, M., Boni Vicari, M., Burt, A., Calders, K., Lewis, S. L., Raumonen, P., & Wilkes, P. (2018). Weighing trees with lasers: advances, challenges and opportunities. *Interface focus*, *8*(2), 20170048. https://doi.org/10.1098/rsfs.2017.0048

Disney, M. (2019). Terrestrial LiDAR: a three-dimensional revolution in how we look at trees. *The New phytologist*, *222*(4), 1736–1741. https://doi.org/10.1111/nph.15517

Edelsbrunner, H., & Mücke, E. P. (1992). Three-dimensional alpha shapes. *Proceedings of the 1992 Workshop on Volume Visualization*, 75–82. https://doi.org/10.1145/147130.147153

Esmoris, A. M., Yermo, M., Weiser, H., Winiwarter, L., Hofle, B., & Rivera, F. F. (2022). Virtual LiDAR Simulation as a High Performance Computing Challenge: Toward HPC HELIOS++. *IEEE Access*, *10*, 105052–105073. https://doi.org/10.1109/ACCESS.2022.3211072

Fang, H., Baret, F., Plummer, S., & Schaepman–Strub, G. (2019). An Overview of Global Leaf Area Index (LAI): Methods, Products, Validation, and Applications. *Reviews of Geophysics*, *57*(3), 739–799. https://doi.org/10.1029/2018RG000608

Hackenberg, J. (2021). SimpleForest. Retrieved 2021-01-06, from https://simpleforest.org/

Hackenberg, J., Morhart, C., Sheppard, J., Spiecker, H., & Disney, M. (2014). Highly Accurate Tree Models Derived from Terrestrial Laser Scan Data: A Method Description. *Forests*, *5*(5), 1069–1105. https://doi.org/10.3390/f5051069

Heuvelink, E., Bakker, M. J., Elings, A., Kaarsemaker, R. C., & Marcelis, L. (2005). Effect of Leaf Area on Tomato Yield. *Acta Horticulturae*, (691), 43–50. https://doi.org/10.17660/ActaHortic.2005.691.2

Jackson, T., Shenkin, A., Moore, J., Bunce, A., van Emmerik, T., Kane, B., Burcham, D., James, K., Selker, J., Calders, K., Origo, N., Disney, M., Burt, A., Wilkes, P., Raumonen, P., Gonzalez de Tanago Menaca, J., Lau, A., Herold, M., Goodman, R. C., … Malhi, Y. (2019). An architectural understanding of natural sway frequencies in trees. *Journal of the Royal Society, Interface*, *16*(155), 20190116. https://doi.org/10.1098/rsif.2019.0116

Jacobs, M., Rais, A., & Pretzsch, H. (2021). How drought stress becomes visible upon detecting tree shape using terrestrial laser scanning (TLS). *Forest Ecology and Management*, *489*, 118975. https://doi.org/10.1016/j.foreco.2021.118975

Kalisperakis, I., Stentoumis, C., Grammatikopoulos, L., & Karantzalos, K. (2015). Leaf Area Index Estimation in Vineyards from UAV Hyperspectral Data, 2D Image Mosaics and 3D Canopy Surface Models. *The International Archives of the Photogrammetry, Remote Sensing and Spatial Information Sciences*, *XL-1/W4*, 299–303. https://doi.org/10.5194/isprsarchives-XL-1-W4-299-2015

Kattenborn, T., Richter, R., Guimarães-Steinicke, C., Feilhauer, H., & Wirth, C. (2022). Anglecam: Predicting the temporal variation of leaf angle distributions from image series with deep

learning. *Methods in Ecology and Evolution*, *13*(11), 2531–2545. https://doi.org/https://doi.org/10.1111/2041-210X.13968

Kazhdan, M., Bolitho, M., & Hoppe, H. (2006). Poisson Surface Reconstruction. In A. Sheffer & K. Polthier (Eds.), *Symposium on geometry processing*. The Eurographics Association. https://doi.org/10.2312/SGP/SGP06/061-070

Kükenbrink, D., Schneider, F. D., Leiterer, R., Schaepman, M. E., & Morsdorf, F. (2017). Quantification of hidden canopy volume of airborne laser scanning data using a voxel traversal algorithm. *Remote Sensing of Environment*, *194*, 424–436. https://doi.org/10.1016/j.rse.2016.10.023

Lecigne, B., Delagrange, S., & Taugourdeau, O. (2021). Annual Shoot Segmentation and Physiological Age Classification from TLS Data in Trees with Acrotonic Growth. *Forests*, *12*(4), 391. https://doi.org/10.3390/f12040391

Levin, D. (2004). Mesh-independent surface interpolation. In G. Brunnett, B. Hamann, H. Müller & L. Linsen (Eds.), *Geometric modeling for scientific visualization* (pp. 37–49). Springer Berlin Heidelberg. https://doi.org/10.1007/978-3-662-07443-5_3

Liang, X., Kankare, V., Hyyppä, J., Wang, Y., Kukko, A., Haggrén, H., Yu, X., Kaartinen, H., Jaakkola, A., Guan, F., Holopainen, M., & Vastaranta, M. (2016). Terrestrial laser scanning in forest inventories. *ISPRS Journal of Photogrammetry and Remote Sensing*, *115*, 63–77. https://doi.org/10.1016/j.isprsjprs.2016.01.006

Liu, J., Skidmore, A. K., Wang, T., Zhu, X., Premier, J., Heurich, M., Beudert, B., & Jones, S. (2019). Variation of leaf angle distribution quantified by terrestrial LiDAR in natural European beech forest. *ISPRS Journal of Photogrammetry and Remote Sensing*, *148*, 208–220. https://doi.org/10.1016/j.isprsjprs.2019.01.005

Liu, X., Ma, Q., Wu, X., Hu, T., Liu, Z., Liu, L., Guo, Q., & Su, Y. (2022). A novel entropy-based method to quantify forest canopy structural complexity from multiplatform lidar point clouds. *Remote Sensing of Environment*, *282*, 113280. https://doi.org/10.1016/j.rse.2022.113280

Mason, P., Manton, M., Harrison, D., Belward, A., Thomas, A., Dawson, A., Allali, A., Church, J., Clarke, R., Eyre, J., Folland, C., Gould, W., Haeberli, W., Harrison, S., Karl, T. R., Maurer, T., Parker, D., Proffitt, M., Quegan, S., & Verstraete, M. (2003). The Second Report on the Adequacy of the Global Observing Systems for Climate in Support of the UNFCCC.

Moon, T., Choi, H., Kim, D., Hwang, I., Kim, J., Shin, J., & Son, J. E. (2022). Autonomous construction of parameterizable 3D leaf models from scanned sweet pepper leaves with deep generative networks [diac015]. *in silico Plants*, *4*(2). https://doi.org/10.1093/insilicoplants/diac015

Morel, J., Bac, A., & Kanai, T. (2020). Segmentation of unbalanced and in-homogeneous point clouds and its application to 3D scanned trees. *The Visual Computer*, *36*(10-12), 2419–2431. https://doi.org/10.1007/s00371-020-01966-7

Morsdorf, F., Eck, C., Zgraggen, C., Imbach, B., Schneider, F. D., & Kükenbrink, D. (2017). Uav-based lidar acquisition for the derivation of high-resolution forest and ground information. *The Leading Edge*, *36*, 566–570. https://doi.org/10.1190/tle36070566.1

PDAL Contributors. (2022). PDAL Point Data Abstraction Library. https://doi.org/10.5281/zenodo.2616780

Pimont, F., Allard, D., Soma, M., & Dupuy, J.-L. (2018). Estimators and confidence intervals for plant area density at voxel scale with T-LiDAR. *Remote Sensing of Environment*, *215*, 343–370. https://doi.org/10.1016/j.rse.2018.06.024

Pirk, S., Niese, T., Hädrich, T., Benes, B., & Deussen, O. (2014). Windy trees. *ACM Transactions on Graphics*, *33*(6), 1–11. https://doi.org/10.1145/2661229.2661252

Puttonen, E., Briese, C., Mandlburger, G., Wieser, M., Pfennigbauer, M., Zlinszky, A., & Pfeifer, N. (2016). Quantification of Overnight Movement of Birch (Betula pendula) Branches and Foliage with Short Interval Terrestrial Laser Scanning. *Frontiers in plant science*, *7*, 222. https://doi.org/10.3389/fpls.2016.00222

Puttonen, E., Lehtomäki, M., Litkey, P., Näsi, R., Feng, Z., Liang, X., Wittke, S., Pandžić, M., Hakala, T., Karjalainen, M., & Pfeifer, N. (2019). A Clustering Framework for Monitoring Circadian Rhythm in Structural Dynamics in Plants From Terrestrial Laser Scanning Time Series. *Frontiers in plant science*, *10*, 486. https://doi.org/10.3389/fpls.2019.00486

py4dgeo Development Core Team. (2022). *py4dgeo: library for change analysis in 4D point clouds.* (Version 0.5.0). Retrieved 2023-05-11, from https://github.com/3dgeo-heidelberg/py4dgeo

Rabbani, T., van den Heuvel, F., & Vosselman, G. (2006). Segmentation of point clouds using smoothness constraints. In H. Maas & D. Schneider (Eds.), *ISPRS 2006 : Proceedings of the ISPRS Commission V Symposium Vol. 35, Part 6: Image Engineering and Vision Metrology, Dresden, Germany 25-27 September 2006"* (pp. 248–253). Internatonal Society for Photogrammetry; Remote Sensing (ISPRS).

Raumonen, P., & Åkerblom, M. (2022). InverseTampere/TreeQSM: Version 2.4.1. https://doi.org/10.5281/zenodo.844625

Raumonen, P., Kaasalainen, M., Åkerblom, M., Kaasalainen, S., Kaartinen, H., Vastaranta, M., Holopainen, M., Disney, M., & Lewis, P. (2013). Fast Automatic Precision Tree Models from Terrestrial Laser Scanner Data. *Remote Sensing*, *5*(2), 491–520. https://doi.org/10.3390/rs5020491

Ridel, B., Guennebaud, G., Reuter, P., & Granier, X. (2015). Parabolic-cylindrical moving least squares surfaces. *Computers & Graphics*, *51*, 60–66. https://doi.org/10.1016/j.cag.2015.05.006

RIEGL LMS. (2017). RIEGL VZ-400: 3D Terrestrial Laser Scanner with Online Waveform Processing. Retrieved 2023-01-06, from http://www.riegl.com/uploads/tx_pxpriegldownloads/10_DataSheet_VZ-400_2017-06-14.pdf

RIEGL LMS. (2022a). RIEGL VZ-2000i: Long Range, Very High Speed 3D Laser Scanner. Retrieved 2023-05-13, from http://www.riegl.com/uploads/tx_pxpriegldownloads/RIEGL_VZ-2000i_Datasheet_2022-09-27.pdf

RIEGL LMS. (2022b). RiSCAN PRO (version 2.12.1). Retrieved 2023-01-06, from http://www.riegl.com/uploads/tx_pxpriegldownloads/RiSCAN-PRO_DataSheet_2022-10-07.pdf

RIEGL LMS. (2023). RIEGL VUX-1UAV^{22}: Lightweight UAV Laser Scanner with Online Waveform Processing. Retrieved 2023-05-13, from http://www.riegl.com/uploads/tx_pxpriegldownloads/RIEGL_VUX-1UAV-22_Datasheet_2023-04-25.pdf

Running, S. W., & Coughlan, J. C. (1988). A general model of forest ecosystem processes for regional applications I. Hydrologic balance, canopy gas exchange and primary production processes. *Ecological Modelling*, *42*(2), 125–154. https://doi.org/10.1016/0304-3800(88)90112-3

Rusu, R. B., Márton, Z.-C., Blodow, N., Dolha, M. E., & Beetz, M. (2008). Towards 3D Point cloud based object maps for household environments. *Robotics Auton. Syst.*, *56*, 927–941. https://doi.org/10.1016/j.robot.2008.08.005

Seidel, D., Fleck, S., & Leuschner, C. (2012). Analyzing forest canopies with ground-based laser scanning: A comparison with hemispherical photography. *Agricultural and Forest Meteorology*, *154-155*, 1–8. https://doi.org/10.1016/j.agrformet.2011.10.006

Skidmore, A. K., Coops, N. C., Neinavaz, E., Ali, A., Schaepman, M. E., Paganini, M., Kissling, W. D., Vihervaara, P., Darvishzadeh, R., Feilhauer, H., Fernandez, M., Fernández, N., Gorelick, N., Geijzendorffer, I., Heiden, U., Heurich, M., Hobern, D., Holzwarth, S., Muller-Karger, F. E., … Wingate, V. (2021). Priority list of biodiversity metrics to observe from space. *Nature ecology & evolution*, *5*(7), 896–906. https://doi.org/10.1038/s41559-021-01451-x

Stovall, A. E. L., Masters, B., Fatoyinbo, L., & Yang, X. (2021). TLSLeAF: automatic leaf angle estimates from single-scan terrestrial laser scanning. *The New phytologist*, *232*(4), 1876–1892. https://doi.org/10.1111/nph.17548

Strachan, I. B., Stewart, D. W., & Pattey, E. (2005). Determination of Leaf Area Index in Agricultural Systems. In J. L. Hatfield & J. M. Baker (Eds.), *Micrometeorology in Agricultural Systems* (pp. 179–198). American Society of Agronomy, Crop Science Society of America, and Soil Science Society of America. https://doi.org/10.2134/agronmonogr47.c9

Tadrist, L., Saudreau, M., Hémon, P., Amandolese, X., Marquier, A., Leclercq, T., & de Langre, E. (2018). Foliage motion under wind, from leaf flutter to branch buffeting. *Journal of the Royal Society, Interface*, *15*(142). https://doi.org/10.1098/rsif.2018.0010

Vaaja, M. T., Virtanen, J.-P., Kurkela, M., Lehtola, V., Hyyppä, J., & Hyyppä, H. (2016). The Effect of Wind on Tree Stem Parameter Estimation Using Terrestrial Laser Scanning. *ISPRS Annals of the Photogrammetry, Remote Sensing and Spatial Information Sciences*, *III-8*, 117–122. https://doi.org/10.5194/isprsannals-III-8-117-2016

Vicari, M. B., Pisek, J., & Disney, M. (2019). New estimates of leaf angle distribution from terrestrial LiDAR: Comparison with measured and modelled estimates from nine broadleaf tree species. *Agricultural and Forest Meteorology*, *264*, 322–333. https://doi.org/10.1016/j.agrformet.2018.10.021

Vincent, G., Pimont, F., & Verley, P. (2021). Various PAD/LAD estimators implemented in AMAPVox 1.8. https://doi.org/10.23708/1AJNMP

Vincent, G., Antin, C., Laurans, M., Heurtebize, J., Durrieu, S., Lavalley, C., & Dauzat, J. (2017). Mapping plant area index of tropical evergreen forest by airborne laser scanning. A cross-validation study using LAI2200 optical sensor. *Remote Sensing of Environment*, *198*, 254–266. https://doi.org/10.1016/j.rse.2017.05.034

Wang, D., Hollaus, M., & Pfeifer, N. (2017). Feasibility of Machine Learning Methods for Separating Wood and Leaf Points from Terrestrial Laser Scanning Data. *ISPRS Annals of the Photogrammetry, Remote Sensing and Spatial Information Sciences*, *IV-2/W4*, 157–164. https://doi.org/10.5194/isprs-annals-IV-2-W4-157-2017

Wang, D. (2020). Unsupervised semantic and instance segmentation of forest point clouds. *ISPRS Journal of Photogrammetry and Remote Sensing*, *165*, 86–97. https://doi.org/10.1016/j.isprsjprs.2020.04.020

Wang, D., Puttonen, E., & Casella, E. (2022). PlantMove: A tool for quantifying motion fields of plant movements from point cloud time series. *International Journal of Applied Earth Observation and Geoinformation*, *110*, 102781. https://doi.org/10.1016/j.jag.2022.102781

Weber, J., & Penn, J. (1995). Creation and rendering of realistic trees. In S. G. Mair & R. Cook (Eds.), *Proceedings of the 22nd annual conference on Computer graphics and interactive techniques - SIGGRAPH '95* (pp. 119–128). ACM Press. https://doi.org/10.1145/218380.218427

Weinmann, M., Urban, S., Hinz, S., Jutzi, B., & Mallet, C. (2015). Distinctive 2D and 3D features for automated large-scale scene analysis in urban areas. *Computers & Graphics*, *49*, 47–57. https://doi.org/10.1016/j.cag.2015.01.006

Wilkes, P., Lau, A., Disney, M., Calders, K., Burt, A., Gonzalez de Tanago, J., Bartholomeus, H., Brede, B., & Herold, M. (2017). Data acquisition considerations for Terrestrial Laser Scanning of forest plots. *Remote Sensing of Environment*, *196*, 140–153. https://doi.org/10.1016/j.rse.2017.04.030

Winiwarter, L., Anders, K., Schröder, D., & Höfle, B. (2022a). Virtual Laser Scanning of Dynamic Scenes Created from Real 4D Topographic Point Cloud Data. *ISPRS Annals of the Photogrammetry, Remote Sensing and Spatial Information Sciences*, *V-2-2022*, 79–86. https://doi.org/10.5194/isprs-annals-V-2-2022-79-2022

Winiwarter, L., Esmorís Pena, A. M., Weiser, H., Anders, K., Martínez Sánchez, J., Searle, M., & Höfle, B. (2022b). Virtual laser scanning with HELIOS++: A novel take on ray tracing-based simulation of topographic full-waveform 3D laser scanning. *Remote Sensing of Environment*, *269*, 112772. https://doi.org/10.1016/j.rse.2021.112772

Wu, B., Zheng, G., Chen, Y., & Yu, D. (2021). Assessing inclination angles of tree branches from terrestrial laser scan data using a skeleton extraction method. *International Journal of Applied Earth Observation and Geoinformation*, *104*, 102589. https://doi.org/10.1016/j.jag.2021.102589

Xi, Z., Hopkinson, C., Rood, S. B., & Peddle, D. R. (2020). See the forest and the trees: Effective machine and deep learning algorithms for wood filtering and tree species classification from terrestrial laser scanning. *ISPRS Journal of Photogrammetry and Remote Sensing*, *168*, 1–16. https://doi.org/10.1016/j.isprsjprs.2020.08.001

Xu, L., Yang, Z., Ding, W., & Buck-Sorlin, G. (2020). Physics-based algorithm to simulate tree dynamics under wind load. *International Journal of Agricultural and Biological Engineering*, *13*(2), 26–32. https://doi.org/10.25165/j.ijabe.20201302.4967

Yan, D.-M., Wintz, J., Mourrain, B., Wang, W., Boudon, F., & Godin, C. (2009). Efficient and robust tree model reconstruction from laser scanned data points. *In Proceedings of the 11th IEEE International conference on Computer-Aided Design and Computer Graphics*, 572–576.

Yan, G., Hu, R., Luo, J., Weiss, M., Jiang, H., Mu, X., Xie, D., & Zhang, W. (2019). Review of indirect optical measurements of leaf area index: Recent advances, challenges, and perspectives. *Agricultural and Forest Meteorology*, *265*, 390–411. https://doi.org/10.1016/j.agrformet.2018.11.033

You, H., Li, S., Ma, L., & Di Wang. (2022). Leaf Area Index Retrieval for Broadleaf Trees by Envelope Fitting Method Using Terrestrial Laser Scanning Data. *IEEE Geoscience and Remote Sensing Letters*, *19*, 1–5. https://doi.org/10.1109/LGRS.2022.3214427

Yun, T., An, F., Li, W., Sun, Y., Cao, L., & Xue, L. (2016). A Novel Approach for Retrieving Tree Leaf Area from Ground-Based LiDAR. *Remote Sensing*, *8*(11), 942. https://doi.org/10.3390/rs8110942

Yun, T., Cao, L., An, F., Chen, B., Xue, L., Li, W., Pincebourde, S., Smith, M. J., & Eichhorn, M. P. (2019). Simulation of multi-platform LiDAR for assessing total leaf area in tree crowns. *Agricultural and Forest Meteorology*, *276-277*, 107610. https://doi.org/10.1016/j.agrformet.2019.06.009

Zhang, B., Wang, X., Yuan, X., An, F., Zhang, H., Zhou, L., Shi, J., & Yun, T. (2022). Simulating Wind Disturbances over Rubber Trees with Phenotypic Trait Analysis Using Terrestrial Laser Scanning. *Forests*, *13*(8), 1298. https://doi.org/10.3390/f13081298

Zhou, J., Wei, H., Zhou, G., & Song, L. (2019). Separating Leaf and Wood Points in Terrestrial Laser Scanning Data Using Multiple Optimal Scales. *Sensors (Basel, Switzerland)*, *19*(8). https://doi.org/10.3390/s19081852

Zhou, Q.-Y., Park, J., & Koltun, V. (2018). Open3D: A modern library for 3D data processing. *arXiv:1801.09847*.

Zhu, X., Liu, J., Skidmore, A. K., Premier, J., & Heurich, M. (2020). A voxel matching method for effective leaf area index estimation in temperate deciduous forests from leaf-on and leaf-off airborne LiDAR data. *Remote Sensing of Environment*, *240*, 111696. https://doi.org/10.1016/j.rse.2020.111696

Zlinszky, A., Molnár, B., & Barfod, A. S. (2017). Not All Trees Sleep the Same - High Temporal Resolution Terrestrial Laser Scanning Shows Differences in Nocturnal Plant Movement. *Frontiers in plant science*, *8*, 1814. https://doi.org/10.3389/fpls.2017.01814